Monthly Notices
of the
ROYAL ASTRONOMICAL SOCIETY

MNRAS **491,** 2465–2480 (2020)
Advance Access publication 2019 November 4

doi:10.1093/mnras/stz3081
FERMILAB-PUB-20-070-AE
ACCEPTED

# Discovery of a nearby 1700 km s$^{-1}$ star ejected from the Milky Way by Sgr A*

Sergey E. Koposov [1,2★] Douglas Boubert [3] Ting S. Li [4,5,6,7†] Denis Erkal [8] Gary S. Da Costa [9] Daniel B. Zucker,[10,11] Alexander P. Ji,[4] Kyler Kuehn,[12,13] Geraint F. Lewis [14] Dougal Mackey,[9,15] Jeffrey D. Simpson [16] Nora Shipp,[6,7,17] Zhen Wan [14] Vasily Belokurov [2] Joss Bland-Hawthorn [14,15] Sarah L. Martell [15,16] Thomas Nordlander [9,15] Andrew B. Pace [18] Gayandhi M. De Silva,[13,15] Mei-Yu Wang[1] and (S$^5$ collaboration)

*Affiliations are listed at the end of the paper*

Accepted 2019 October 30. Received 2019 October 30; in original form 2019 July 26

## ABSTRACT

We present the serendipitous discovery of the fastest main-sequence hyper-velocity star (HVS) by the Southern Stellar Stream Spectroscopic Survey (S$^5$). The star S5-HVS1 is a ∼2.35 M$_\odot$ A-type star located at a distance of ∼9 kpc from the Sun and has a heliocentric radial velocity of 1017 ± 2.7 km s$^{-1}$ without any signature of velocity variability. The current 3D velocity of the star in the Galactic frame is 1755 ± 50 km s$^{-1}$. When integrated backwards in time, the orbit of the star points unambiguously to the Galactic Centre, implying that S5-HVS1 was kicked away from Sgr A* with a velocity of ∼1800 km s$^{-1}$ and travelled for 4.8 Myr to its current location. This is so far the only HVS confidently associated with the Galactic Centre. S5-HVS1 is also the first hyper-velocity star to provide constraints on the geometry and kinematics of the Galaxy, such as the Solar motion $V_{y,\odot} = 246.1 \pm 5.3$ km s$^{-1}$ or position $R_0 = 8.12 \pm 0.23$ kpc. The ejection trajectory and transit time of S5-HVS1 coincide with the orbital plane and age of the annular disc of young stars at the Galactic Centre, and thus may be linked to its formation. With the S5-HVS1 ejection velocity being almost twice the velocity of other hyper-velocity stars previously associated with the Galactic Centre, we question whether they have been generated by the same mechanism or whether the ejection velocity distribution has been constant over time.

**Key words:** stars: kinematics and dynamics – Galaxy: centre – Galaxy: fundamental parameters.

## 1 INTRODUCTION

Throughout the last 100 yr of studying our Galaxy, there was always a prominent niche in identifying fast moving stars on the sky or in 3D. One of the first studies of high-velocity stars was the PhD thesis by Oort (1926) who put a boundary between high-velocity and low-velocity stars at 63 km s$^{-1}$. Initially, the searches for fast moving stars were focused on using the proper motions (van Maanen 1917; Luyten 1979) because these were easier to obtain in larger numbers than radial velocities. Due to the fact that the tangential velocities are distance dependent, these searches provided us with some of the first large samples of nearby and Milky Way (MW) halo stars (Barnard 1916; Eggen & Greenstein 1967; Eggen 1983).

When larger numbers of radial velocities began to be analysed in the 1950s–1960s (Kennedy & Przybylski 1963) the term 'high velocity star' was used to refer to the stars with space velocities of $\gtrsim$100 km s$^{-1}$ (Keenan & Keller 1953), where those stars were mostly MW stellar halo stars (Eggen, Lynden-Bell & Sandage 1962). Around the same time, another type of high velocity object emerged – the runaway OB stars (Blaauw & Morgan 1954). These stars did not have extreme space velocities, but instead were just offset from the expected velocity of the disc by 100–200 km s$^{-1}$. Some stars were later found in the MW halo (Greenstein & Sargent 1974) with velocities up to 200 km s$^{-1}$. The mechanism proposed for the formation of such high-velocity stars involves either a

★ E-mail: skoposov@cmu.edu
† Hubble Fellow.


Fermi Research Alliance, LLC under Contract No. DE-AC02-07CH11359 with the U.S. Department of Energy, Office of Science, Office of High Energy Physics.

supernovae explosion in a binary (Blaauw 1961) or ejection due to encounters in clusters (Poveda, Ruiz & Allen 1967).

For a while these pathways seemed to be the most promising for creating fast moving stars in the Galaxy with velocities potentially up to the escape speed. However, Hills (1988) proposed an entirely new mechanism of creating fast moving stars with velocities of 1000 $\mathrm{km\,s^{-1}}$ and above (labelled hyper-velocity stars, HVS) by interaction of a stellar binary with a supermassive black hole (SMBH) in the centres of galaxies. This mechanism was almost forgotten until the early 2000s, when Yu & Tremaine (2003) analysed the ejection mechanism from single and binary SMBHs and Brown et al. (2005) identified a star in the Milky Way halo at a distance of 40–70 kpc with a total velocity of $\sim$700 $\mathrm{km\,s^{-1}}$, well above the escape velocity at such a distance. This discovery spurred a renewed interest in hyper-velocity stars (Edelmann et al. 2005; Hirsch et al. 2005; Heber et al. 2008; Przybilla et al. 2008) and led to dedicated searches, resulting in multiple new HVS (Zheng et al. 2014; Huang et al. 2017; Irrgang et al. 2019) and candidate HVS (see Brown 2015 for a detailed overview and more references).

The most recent part of the story is the arrival of *Gaia* data (Gaia Collaboration et al. 2016), in particular Data Release 2 (Gaia Collaboration et al. 2018) that provided high accuracy proper motions, and thus enabled new discoveries (Shen et al. 2018), potential discoveries (Bromley et al. 2018; Hattori et al. 2018a; Marchetti, Rossi & Brown 2018; Boubert et al. 2019) as well as detailed studies of the HVS origins (Boubert et al. 2018; Brown et al. 2018; Irrgang, Kreuzer & Heber 2018; Erkal et al. 2019). One of the key conclusions from these studies is that despite the large number of HVS candidates, only a handful of these appear to be actually unbound from the Galaxy and consistent with ejection from the Galactic Centre (GC).

Whilst the extreme speed of several of the HVS in the outer halo is seemingly unexplainable without the Hills mechanism, the uncertainties on their distances and proper motions are such that they cannot be tracked back precisely to the GC. The most convincing association to date is the star J01020100−7122208, identified by Massey et al. (2018) as a bound runaway star that in a particular choice of potential tracked back to the GC; however, the low 3D velocity of 296 $\mathrm{km\,s^{-1}}$ does not preclude a more standard origin. There is not yet an example of an HVS that unequivocally tracks back to the GC, and thus no smoking gun for a GC Hills mechanism ejection. The power of HVS as probes of the Galactic potential (Gnedin et al. 2005) and the orbit of the Sun (Hattori, Valluri & Castro 2018b) is contingent on an unambiguous GC origin, and thus it is of paramount importance that such a smoking gun is found.

In this paper, we present the discovery of a new nearby unbound HVS that can be unambiguously traced back to the GC. The star is named S5-HVS1 as it was found in the Southern Stellar Stream Spectroscopic Survey ($S^5$; Li et al. 2019).

The structure of the paper is as follows. In Section 2, we briefly introduce the $S^5$ data that was used to identify the S5-HVS1 star and the search for HVS stars in $S^5$ data. In Section 3, we look at the spectroscopic and photometric properties of S5-HVS1. In Section 4, we analyse the kinematics of the star and its possible origin in the Galaxy. In Section 5, we focus on the GC as a source of S5-HVS1 as well as inferences we can make on the Galactic potential, distance and velocity of the Sun with respect to the GC. We discuss S5-HVS1 in more detail in Section 6 by comparing it to other HVS, as well as examining HVS ejection mechanisms. Our conclusions are given in Section 7.

## 2 DATA

The $S^5$ project is a survey devoted to the observation of stellar streams in the Southern hemisphere (Li et al. 2019). The survey is being conducted on the 3.9 m Anglo-Australian Telescope (AAT) with the Two-degree Field (2dF) fibre positioner feeding the AAOmega dual arm spectrograph (Lewis et al. 2002; Sharp et al. 2006). $S^5$ uses low (580V, $R \sim 1300$) and high (1700D, $R \sim 10\,000$) resolution gratings in the blue and red wavelength ranges, respectively, covering the Balmer break region (3800 Å $< \lambda <$ 5800 Å) in the blue and IR calcium triplet (8400 Å $< \lambda <$ 8800 Å) in the red. The survey is ongoing, but by early 2019, it had observed 110 fields spread across $\sim$330 $\mathrm{deg^2}$ and $\sim$40 000 targets. For details, we refer the reader to the Li et al. (2019) paper, while providing here only the key aspects of the survey.

$S^5$ is primarily targeting stellar stream candidate members, selected based on photometric information from the Dark Energy Survey (DES) DR1 (Abbott et al. 2018) and proper motion and parallax information from *Gaia* DR2 (Gaia Collaboration et al. 2016, 2018). To fill all the 392 fibres of the spectrograph other target classes are observed, including low-redshift galaxy candidates, white dwarfs (WDs), and metal-poor stars, etc. The survey specifically targets blue stars that could be Blue Horizontal Branch (BHB) stars, Blue Stragglers (BS), or RR Lyrae stars at a large range of distances. The selection used by $S^5$ for the BHB/BS stars is $-0.4 < (g-r) < 0.1$ and $parallax < 3 * parallax\_error + 0.2$, combined with the star–galaxy separation criteria using $astrometric\_excess\_noise$ quantities from *Gaia* (Koposov, Belokurov & Torrealba 2017; Lindegren et al. 2018) and $wavg\_spread\_model$ quantities from DES (see equations 1–3 in Li et al. 2019). At the time of writing, the $S^5$ catalogue contains spectra of $\sim$3500 blue faint objects. While many of them end up being quasars (see Li et al. 2019), $\gtrsim$2200 of them are likely BHB/BS/WD stars.

The data processing of the $S^5$ data includes standard data reduction steps by the AAT pipeline, followed by spectral modelling by the RVSPECFIT[1] software in order to determine the radial velocities and stellar atmospheric parameters.

### 2.1 HVS star search

While identifying hyper-velocity stars was not a main goal of the $S^5$ survey, the catalogue of radial velocities (RVs) and spectral fits was inspected for stars with velocities larger than 800 $\mathrm{km\,s^{-1}}$. The majority of objects with such high RVs were spurious measurements caused by either sky subtraction residuals and/or low signal-to-noise spectra; however, the search identified a single bright ($G \sim 16$) star with the *Gaia* DR2 `source_id` 6513109241989477504 and $(\alpha, \delta) = (343.715345^\circ, -51.195607^\circ)$, located in the field of the Jhelum stellar stream, a new stellar stream found in the DES (Shipp et al. 2018). This star had a confident radial velocity measurement of $\sim$1020 $\mathrm{km\,s^{-1}}$, making it one of the fastest moving stars known in the Galaxy. The radial velocity of this star alone, irrespective of the distance, is enough to make the star unbound to the Galaxy (see e.g. Kafle et al. 2014). We label this star S5-HVS1.[2] In the next sections, we focus on the detailed measurements of S5-HVS1 properties: spectroscopic, photometric, and kinematic.

[1] http://github.com/segasai/rvspecfit

[2] S5-HVS1 was previously photometrically identified as a candidate field BHB star by Christlieb et al. (2005) and given the designation HE 2251–5127.

**Table 1.** The measured parameters of the hyper-velocity star S5-HVS1. The top part of the table refers to the measurements from previous surveys, while the bottom one summarizes the measurements presented in the paper. HRV is the heliocentric radial velocity. $D_{\rm hel}$, $D_{\rm hel,GC}$ are heliocentric distance constraints without and with the Galactocentric origin assumption, respectively. $V_{\rm GSR}$, $V_{\rm GSR,GC}$ are the inferred Galactic standard of rest (GSR) velocities of S5-HVS1 determined without and with the Galactocentric origin assumption, respectively. $V_{\rm ej,GC}$ is the expected ejection speed from the GC. $\mu_{\alpha,\rm pred}\cos\delta$, $\mu_{\delta,\rm pred}$ are the predicted proper motions of S5-HVS1 based on the Galactocentric origin.

| Parameter | Value | Unit |
|---|---|---|
| *Gaia* RA | 343.715345 | deg |
| *Gaia* Dec. | −51.195607 | deg |
| *Gaia* DR2 `source_id` | 6513109241989477504 | |
| *Gaia* $\mu_\alpha\cos\delta$ | $35.328 \pm 0.084$ | mas yr$^{-1}$ |
| *Gaia* $\mu_\delta$ | $0.587 \pm 0.125$ | mas yr$^{-1}$ |
| *Gaia* Parallax | $-0.042 \pm 0.091$ | mas |
| *Gaia* RUWE | 1.06284 | |
| $E(B-V)_{\rm SFD}$ | 0.00721 | |
| *Gaia* G | 16.0211 | mag |
| DES $g, r, i, z$ | 15.90, 16.16, 16.40, 16.53 | mag |
| $G_{\rm BP}-G_{\rm RP}$ | $-0.0082 \pm 0.0066$ | mag |
| HRV | $1017.0 \pm 2.7$ | km s$^{-1}$ |
| $T_{\rm eff}$ | $9630 \pm 110$ | K |
| $\log g$ | $4.23 \pm 0.03$ | dex |
| [Fe/H] | $0.29 \pm 0.08$ | dex |
| $\log_{10} D_{\rm hel}/1\,{\rm kpc}$ | $0.936 \pm 0.015$ | |
| $V_{\rm GSR}$ | $1755^{+55}_{-45}$ | km s$^{-1}$ |
| $V_{\rm GSR,GC}$ | $1717.4 \pm 3.5$ | km s$^{-1}$ |
| $V_{\rm ej,GC}$ | $1798.6 \pm 3.1$ | km s$^{-1}$ |
| $D_{\rm hel,GC}$ | $8884 \pm 11$ | pc |
| $\mu_{\alpha,\rm pred}\cos\delta$ | $35.333 \pm 0.080$ | mas yr$^{-1}$ |
| $\mu_{\delta,\rm pred}$ | $0.617 \pm 0.011$ | mas yr$^{-1}$ |

## 3 S5-HVS1 PROPERTIES

In this section, we discuss the key spectroscopic properties of S5-HVS1 as determined from AAT data, as well as all available photometric data. The summary of these measurements is presented in Table 1.

### 3.1 Spectroscopy

The star S5-HVS1 was observed for the first time at the AAT as part of regular S$^5$ observations of the Jhelum stellar stream with the 580V and 1700D gratings on 2018 August 1. The total exposure time was 2 h split into three individual exposures. The combined, reduced spectra for S5-HVS1 are shown in Fig. 1. Based on the spectra, the star appears to be a hot A-type star with prominent broad Balmer and Paschen series and several metal lines like Ca II H/K and Mg II (4481 Å) in the blue and calcium triplet in the red.

Although the stellar spectra of S5-HVS1 in both the blue and red arms were analysed as part of the regular S$^5$ processing (see Li et al. 2019), the analysis treated the blue and red arms separately. For this paper, however, we analyse the blue and red parts of spectra simultaneously in order to better constrain stellar atmospheric parameters. The fitting of stellar spectra is analogous to the procedure described in the *S*$^5$ overview paper and uses the RVSPECFIT, but instead of considering the likelihood function of the red arm or blue arm data separately, we combine them. Specifically, the model for the stellar spectrum uses a combination of global Radial Basis Function interpolation and local linear N–d interpolation of spectra from the PHOENIX-2.0 library (Husser et al. 2013) together with a multiplicative polynomial to deal with the fact that the observed spectra were not flux calibrated (see Koposov et al. 2011):

$$\mathrm{Model}(\lambda|\log g, T_{\rm eff}, [\mathrm{Fe/H}], V) = \left(\sum_{i=0}^{n_p} a_i \lambda^i\right) \times \mathcal{T}\left(\lambda\left[1+\frac{V}{c}\right], \log g, T_{\rm eff}, [\mathrm{Fe/H}]\right).$$

Here, $\lambda$ is the wavelength, the $\mathcal{T}(\lambda, \log g, T_{\rm eff}, [\mathrm{Fe/H}])$ is the interpolated stellar template, $V$ is the radial velocity, $a_i$ are fitted coefficients, and $n_p$ is the degree of the multiplicative polynomial

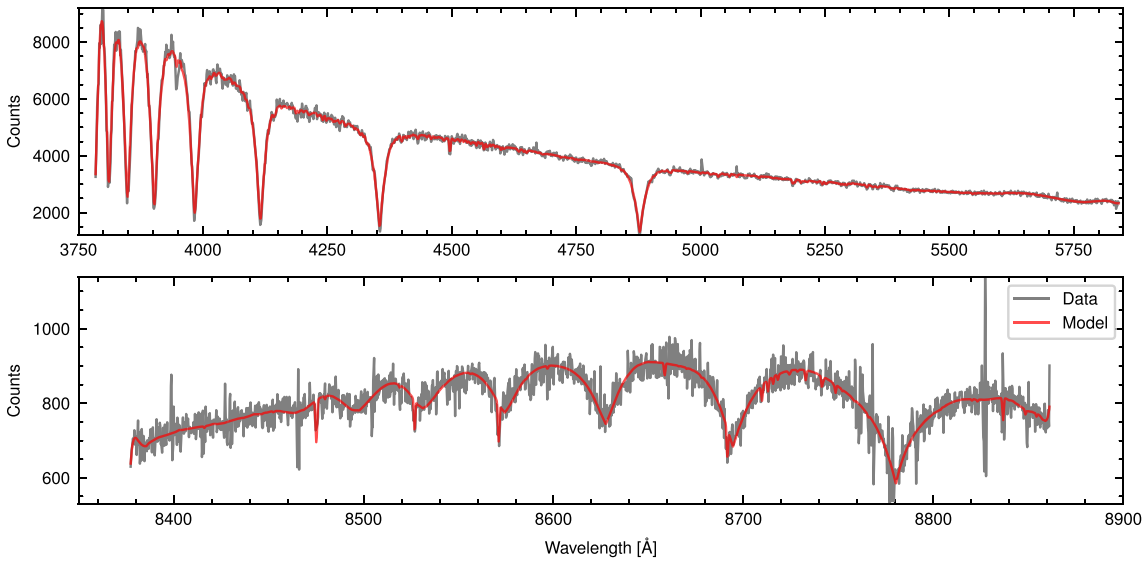


**Figure 1.** The blue and red spectra of S5-HVS1. The grey lines show the spectra from S$^5$ AAT observations, obtained using 580V (top panel) and 1700D (bottom panel) AAT gratings. The red lines show the best-fitting model based on interpolated spectral templates from the PHOENIX library (Husser et al. 2013), which was determined by simultaneous fitting to the blue and red data.

used to correct for continuum normalization.[3] The parameters of the model for the star were then sampled using the parallel tempering Ensemble sampling algorithm (Goodman & Weare 2010; Foreman-Mackey et al. 2013) to determine uncertainties. We adopted non-informative uniform priors on all parameters (i.e. contrary to Li et al. 2019, we did not use the $T_{\rm eff}$ prior based on the colour of the star).

The red curve in Fig. 1 shows the best-fitting spectral model corresponding to the maximum likelihood set of parameters. The stellar atmospheric parameters are effective temperature $T_{\rm eff} = 9630 \pm 110$ K, surface gravity $\log g = 4.23 \pm 0.02$, and high stellar metallicity $[{\rm Fe/H}] = 0.29 \pm 0.08$. We note though that the posterior is bi-modal with two modes at ($T_{\rm eff}$, [Fe/H]) $\sim$ (9500 K, 0.25) and (9700 K, 0.4). This is likely caused by the limitations of the adopted stellar atmosphere grid and interpolation procedure, as the resolution of the PHOENIX grid is 0.5 dex in $\log g$ and [Fe/H] and $\sim$200–500 K in $T_{\rm eff}$. Because of this, the uncertainties on the stellar atmospheric parameters should be mostly systematic. Despite that the measured surface gravity of S5-HVS1 strongly suggests that the star is a main-sequence A-type star as opposed to a BHB star with $\log g \lesssim 3.5$.[4]

While we determined the atmospheric parameters for S5-HVS1 from simultaneous fitting of the red and blue spectra separately from main $S^5$ data processing, the radial velocity measurement for the S5-HVS1 that we will use comes from the main $S^5$ catalogue. The RVs in the catalogue rely only on the red arm of the spectra, as its wavelength calibration and stability are much better controlled due to a higher spectral resolution and the presence of large number of skylines in the science spectra. As discussed in detail in Li et al. (2019), the radial velocities and their uncertainties measured in $S^5$ have been validated with both repeated observations and observations of *Gaia* RVS and APOGEE stars. The uncertainties on the radial velocities also take into account the systematic error floor in our observations of $\sim$0.6 km s$^{-1}$. The heliocentric radial velocity measured for S5-HVS1 by $S^5$ is $1017.0 \pm 2.7$ km s$^{-1}$. The blue arm spectrum provides an independent velocity measurement with a similar value albeit with much larger error bar $1017 \pm 23$ km s$^{-1}$.

### 3.2 Radial velocity variability

The radial velocity of S5-HVS1 is extreme and thus we must consider the possibility that it is due to binary motion. To check this hypothesis, we re-observed the star almost 8 months after the first observation. The first repeated observation was done on 2019 April 6 (MJD 58579.78; i.e. 240 d after the first observation) again using AAT 2dF spectrograph in the same configuration as in the S$^5$ survey. We ensured that S5-HVS1 was assigned to a different fibre and plate from our 2018 observation to rule out any possible fibre-specific effects. The observations were performed in twilight and had an exposure time of only 2 $\times$ 900s and therefore were of lower S/N than standard S$^5$ data.[5] Consequently, the red (1700D) spectrum was not usable, but fortunately the 580V blue spectrum had S/N $\sim$ 3 and we were able to measure a velocity of $V = 1017 \pm 24$ km s$^{-1}$ which is consistent within uncertainties with the original measurement.

We also carried out a further re-observation of S5-HVS1 on 2019 April 26 (MJD 58599.78) using the WiFeS integral field spectrograph (Dopita et al. 2010) on the ANU 2.3m telescope at Siding Spring Observatory. The instrumental set-up employed the B3000 grating that gives resolution $R \sim 3000$ and wavelength coverage of 3500–5600 Å. Two 900s exposures were obtained and the combined reduced spectrum yielded a heliocentric velocity of $1005 \pm 15$ km s$^{-1}$, which is entirely consistent with the other observations. In addition, model atmosphere spectral fits to the WiFeS flux-calibrated spectrum yielded an effective temperature of approximately 10 000 K, and more importantly, a surface gravity $\log g$ of 4.5, confirming the main-sequence star nature of S5-HVS1.

From these additional observations spread over a few months, we can convincingly rule out a binary origin of the high velocity of S5-HVS1, because high binary orbital velocities $\gtrsim$100 km s$^{-1}$ are only expected in binaries with high masses and short periods. It is still possible that S5-HVS1 is part of a long-period binary with a small orbital velocity that is undetectable in a period of $\sim$ a year, but this orbital motion would be negligible compared to the observed RV. Therefore, most of the observed radial velocity must be caused by the motion through the Galaxy.

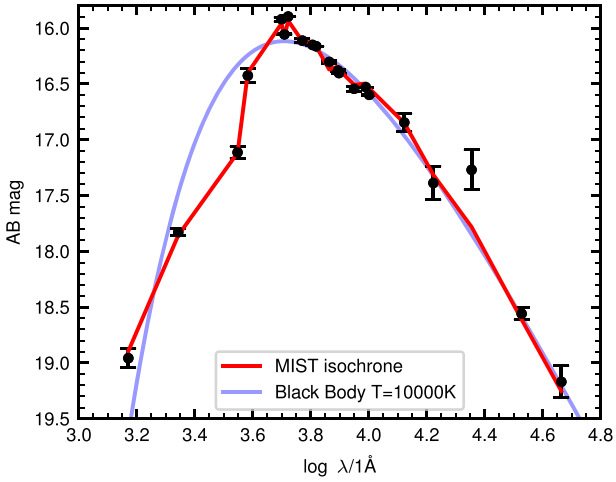


**Figure 2.** Spectral energy distribution (SED) of S5-HVS1 from GALEX, *Gaia*, SkyMapper, DES, 2MASS, and *WISE* photometry. The blue curve is the blackbody spectrum with temperature of 10 000 K. The red line shows the SED from the best-fitting MIST isochrone model. The magnitudes in the data and model were not extinction corrected.

### 3.3 Photometry

S5-HVS1 was targeted by S$^5$ as a blue star with $-0.4 < g - r < 0.1$, which makes it a possible BHB or BS. In this section, we assess the photometric properties of S5-HVS1 by collecting its photometry across multiple wavelengths and fitting these data with an isochrone model.

As S5-HVS1 is quite bright, *Gaia* $G \sim 16$, it is detected in a large number of different surveys. Here, we take the data from DES DR1 (Abbott et al. 2018), 2MASS (Skrutskie et al. 2006), AllWISE (Wright et al. 2010), SkyMapper DR1.1 (Wolf et al. 2018), GALEX (Martin et al. 2005; Bianchi, Shiao & Thilker 2017), and *Gaia* DR2 (Brown et al. 2018; Evans et al. 2018). Fig. 2 shows all

[3]Since the blue arm part of the spectra has a much larger wavelength calibration uncertainty (see Li et al. 2019), when we fit for stellar atmospheric parameters we allowed for a small RV offset between blue and red arms.

[4]We remark that formally the star lies on the BHB side of the $\log g$, $T_{\rm eff}$ distribution shown on fig. 11 of Li et al. (2019). However, the analysis presented in Li et al. (2019) relied only on 1700D data as opposed to combination of 580V and 1700D data that we use here, and is therefore somewhat on different scale.

[5]On 2019 April 6, this star was above airmass $\sim$2 for only 10 min before astronomical twilight.

S5-HVS1 magnitudes (converted when needed from Vega to AB magnitude system), as a function of the effective wavelength of the corresponding filter with standard errors. The SED is clearly indicative of a hot star with temperature ∼10 000 K. The red line shows the photometry from the best-fitting isochrone model in the observed filters that we describe below. The blue line shows a blackbody spectrum with a temperature of 10 000 K.

To model the photometry of S5-HVS1 we use the MIST isochrones (Dotter 2016; Choi et al. 2016, version 1.2) and to interpolate between isochrones we use the ISOCHRONES software (Morton 2015, version 2.0.1).[6] The data that we model are the observed magnitudes $m_i$, where $i$ corresponds to the $i$th band. The isochrones provide us with absolute magnitudes, surface gravities, and effective temperatures as a function of stellar age, mass, metallicity, and band-pass $M(\text{age}, \mathcal{M}, [\text{Fe/H}], i)$. Assuming Gaussian uncertainties of observed magnitudes, our model is

$$m_i \sim \mathcal{N}\big(M(\text{age}, \mathcal{M}, [\text{Fe/H}], i) + 5\log_{10} D_{\rm hel} - 5 + k_i E(B-V), \sqrt{\sigma_i^2 + \sigma_{\rm sys}^2}\big), \quad (1)$$

where $\sigma_i$ is the uncertainty on the magnitude measurement in band $i$, $\sigma_{\rm sys}$ is an additional (systematic) scatter around the model, $D_{\rm hel}$ is the heliocentric distance to the star, and $k_i$ is the extinction coefficient[7] in the filter $i$. On top of the purely photometric model described in equation (1) (we label it Model P), we also consider a model (labelled Model SP) where we complement equation (1) with the constraints on $\log g$, $T_{\rm eff}$, and [Fe/H] from the spectroscopic analysis (see Section 3.1), assuming they are normally distributed (i.e. we multiply the likelihood by Gaussian terms for $\log g$, $T_{\rm eff}$, and [Fe/H]).

We adopt generically uninformative priors for the parameters: uniform distribution on (linear) age $\sim \mathcal{U}(10^5, 1.2 \times 10^{10})$, Salpeter IMF prior for the stellar mass from $\mathcal{M} = 0.1\,{\rm M}_\odot$ to $\mathcal{M} = 5\,{\rm M}_\odot$, uniform prior on metallicity $[\text{Fe/H}] \sim \mathcal{U}(-4, 0.5)$, and a uniform prior on distance modulus $5\log_{10} D_{\rm hel} - 5 \sim \mathcal{U}(10, 20)$ corresponding to a $1/D^2$ spatial density prior from 1 to 100 kpc. For the extinction, we adopt a prior around the Schlegel, Finkbeiner & Davis (1998) value $E(B-V) \sim \mathcal{U}(0.3E_{\rm SFD}, 3E_{\rm SFD})$. The posterior of the model is sampled using the nested sampling MULTINEST algorithm (Feroz & Hobson 2008; Buchner et al. 2014).

The posterior of the model parameters is shown in Fig. 3; blue contours and curves for Model P and green for Model SP. Focusing on the Model P first, we notice that as expected from photometric only data there are considerable degeneracies between mass, age, metallicity, and distance of the star. The summary of parameters for Model P is provided in Table 2. The age of the star is consistent with a broad range of ages up to 500 Myr. The mass of the star is inferred to be $1.9 \pm 0.25\,{\rm M}_\odot$. The distance to the star is constrained to be $\log_{10} \frac{D_{\rm hel}}{1\,{\rm kpc}} = 0.836 \pm 0.083$, putting it in the range of between ∼4.5 and 10 kpc from the Sun. We notice that this distance corresponds to a parallax of $\pi_{\rm phot} \sim 0.14$ mas which is consistent within $2\sigma$ with the negative *Gaia* parallax measurement $\pi_{Gaia} = -0.042 \pm 0.091$ mas that was not used in the fit. The systematic error for the photometry is determined by the model to be $\sigma_{\rm sys} = 0.04 \pm 0.01$, showing that there is no large discrepancy between isochrone models and data.

The match between the data and the isochrone model across the wavelengths is well demonstrated by Fig. 2. Red points with error bars shown on multiple panels of Fig. 3 mark the parameter values measured from spectroscopic analysis of S5-HVS1 (Section 3.1). The measurements from photometric data only are broadly consistent with the spectroscopic analysis, as the error bars overlap with the high probability parts of the posterior. Although there is possibly a small discrepancy in temperature of ∼200 K and/or [Fe/H] of ∼0.2 dex between purely spectroscopic and photometric measurements, we believe this level of disagreement is well within the systematic errors of our spectroscopic and isochrone modelling.

Since the photometric and spectroscopic analyses are consistent, we also show in the figure the posterior from the combination of the spectroscopic and photometric analyses (Model SP) as green contours. As expected, the combination of the data sets shrinks the posteriors considerably, i.e. the combined mass estimate is $2.35 \pm 0.06\,{\rm M}_\odot$ and distance estimate is $\log \frac{D_{\rm hel}}{1\,{\rm kpc}} = 0.936 \pm 0.015$. The posterior estimates for these and other parameters from the Model SP are also provided in Table 2. Throughout the paper, we use both the photometric and photometric+spectroscopic sets of estimates, where we will interpret the photometric-only constraints as being more conservative.[8] As we will discuss in the next section, the kinematics of S5-HVS1 are consistent with ejection from the GC if the star has a very specific heliocentric distance of ∼8.8 kpc. Pink lines on Fig. 3 show the heliocentric distance to the star that is consistent with ejection from the GC (see Section 5), and we remark that this distance agrees perfectly with both the photometric and spectrophotometric analyses.

While the isochrone modelling performed so far did include the horizontal branch phase, the posterior on the stellar parameters indicates that the photometry of S5-HVS1 is inconsistent with it being a BHB star. However, it is still worth specifically addressing the possibility that S5-HVS1 is a BHB, because this is quite feasible given the star's colour of $g - r \sim -0.27$ (most BHB stars have colours of $-0.3 \lesssim g - r \lesssim 0$; Yanny et al. 2000). We therefore perform an independent check to assess the BHB hypothesis by looking at measurements of $g - r$ and $i - z$ colours. This colour combination is known to be sensitive to the surface gravity of stars due to the Paschen break contribution to the $z$-band, and therefore allows us to separate BHB from BS/MS stars (see e.g. Vickers, Grebel & Huxor 2012; Belokurov & Koposov 2016). With colours of $(g - r) = -0.27$ and $(i - z) = -0.13$, S5-HVS1 sits significantly below the line separating the BHB from BS/MS (see the right-hand panel of fig. 11 and equation 5 of Li et al. 2019) further confirming that S5-HVS1 is a main-sequence star. Additionally, when looking at the distribution of surface gravities and effective temperatures (the left-hand panel of fig. 11 of Li et al. 2019) S5-HVS1 lies on the BS side of the distribution. Thus for future analysis, unless specified otherwise, we will adopt the main-sequence–based distance constraints determined in this section.

## 4 KINEMATICS OF S5-HVS1

The extreme radial velocity of S5-HVS1 as measured from the observed spectra makes it one of the fastest stars known in the Galaxy and thus warrants a detailed investigation of its orbit and origin. Summarizing the phase-space information available

[6] For *Gaia* $G_{\rm BP}$, $G_{\rm RP}$ magnitudes we use the band-passes defined by Weiler (2018).

[7] Taken from http://www.mso.anu.edu.au/ brad/filters.html.

[8] In the final stages of preparation of the manuscript, we identified that S5-HVS1 has a distance estimate of $\log_{10} \frac{D_{\rm hel}}{1\,{\rm kpc}} = 0.807 \pm 0.148$ from the STARHORSE code (Anders et al. 2019), which is in very good agreement with our photometric-only measurement.

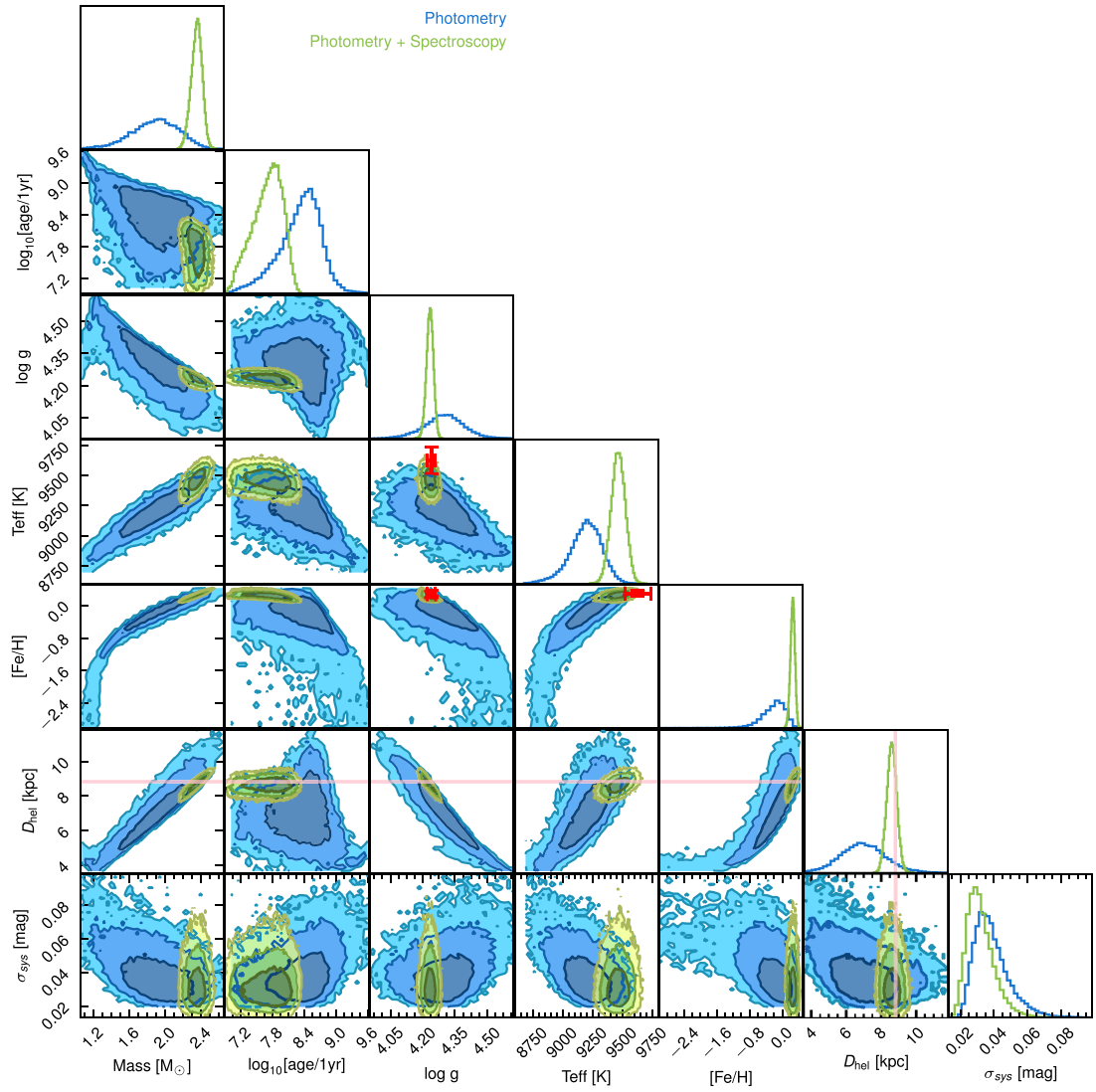


**Figure 3.** The posterior on stellar parameters of S5-HVS1 from fitting MIST isochrones to the SED data only (blue) and the SED data combined with the prior on stellar atmospheric parameters from spectroscopic analysis (green). The red points with error bars are showing the best-fitting measurement of stellar atmospheric parameters from the analysis of the AAT spectra using RVSPECFIT. The pink lines on several panels identify the heliocentric distance to the star that is consistent with the Galactocentric origin (see Section 5). The contour levels in the 2D marginal distributions correspond to the 68 per cent, 95 per cent, and 99.7 per cent of posterior volumes.

for S5-HVS1, the position of the star on the sky is known very precisely, as is the radial velocity. The proper motion of the star is available in the *Gaia* DR2 catalogue and, because of the star's brightness $G \sim 16$, it is also very precise $(\mu_\alpha \cos\delta,\ \mu_\delta) = (35.328 \pm 0.084, 0.587 \pm 0.125)$ mas yr$^{-1}$.[9] The only phase space parameter that is poorly constrained is the heliocentric distance, as discussed in Section 3.3. This is why we expect that most of the orbital inferences for S5-HVS1 should show a 1D degeneracy corresponding to a range of possible heliocentric distances. Even with the more conservative (Model P) distance estimates, it is clear from combining the radial velocity and proper motions that the S5-HVS1 velocity in the Galactic frame is in excess of ∼1200 km s$^{-1}$: $V_{\rm 3D} = 1470^{+166}_{-147}$ km s$^{-1}$.

[9]The astrometry of S5-HVS1 does not seem to be affected by any astrometric problems according to the re-normalized unit weight error (RUWE) (Lindegren et al. 2018), which is ∼1.06.

**Table 2.** The parameters measured from fitting MIST isochrones to the S5-HVS1 SED (Model P) and by combining SED constraints with spectroscopic constraints (Model SP).

| Parameter | Value Photometric | Value Spectro-photometric | Unit |
|---|---|---|---|
| Mass | $1.90^{+0.25}_{-0.28}$ | $2.35^{+0.06}_{-0.06}$ | M$_\odot$ |
| log$_{10}$ age | $8.36^{+0.32}_{-0.46}$ | $7.72^{+0.25}_{-0.33}$ | dex |
| [Fe/H] | $-0.2^{+0.2}_{-0.3}$ | $0.3^{+0.1}_{-0.1}$ | dex |
| m-M | $14.21^{+0.37}_{-0.43}$ | $14.68^{+0.07}_{-0.07}$ | mag |
| $\sigma_{\rm sys}$ | $0.04^{+0.01}_{-0.01}$ | $0.03^{+0.01}_{-0.01}$ | mag |

As a first step in modelling the orbit of S5-HVS1, we perform a backward integration of its current phase space coordinates to infer a possible ejection site of the star. Since the current total velocity of S5-HVS1 is at least 1200 km s$^{-1}$, one of the key questions we

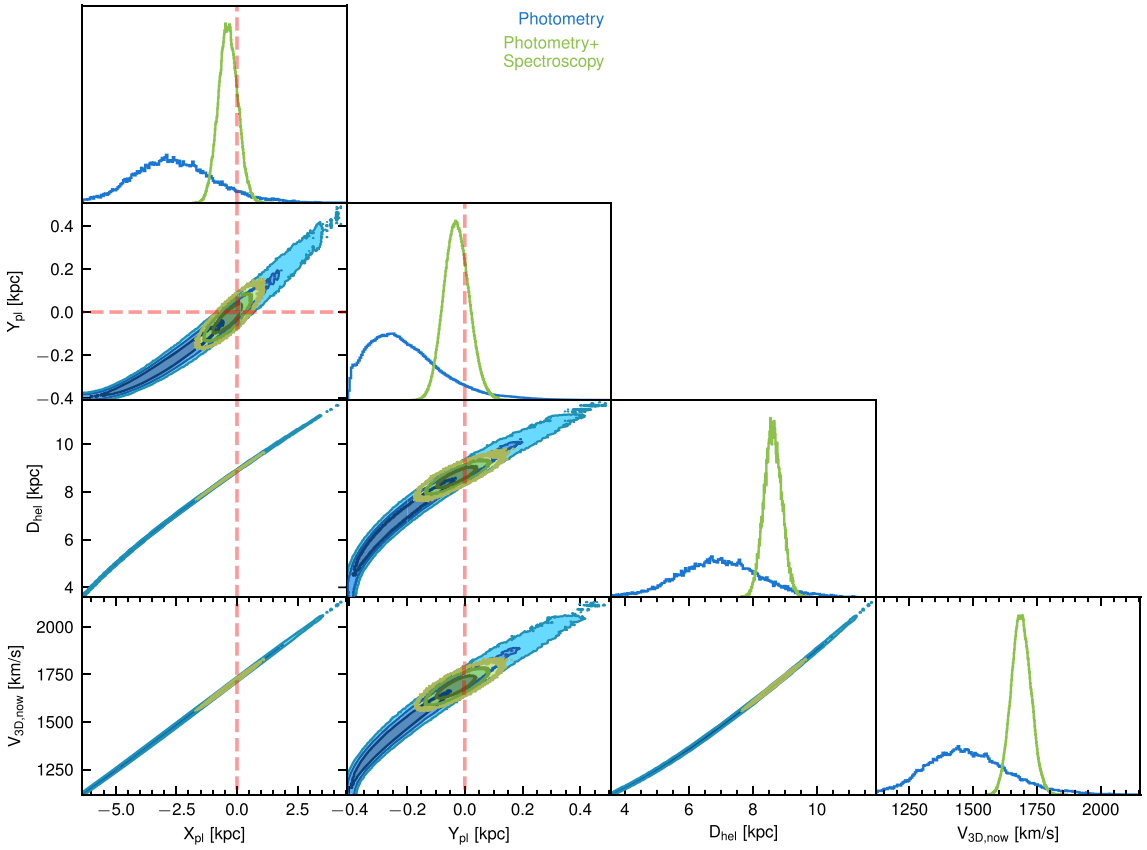


**Figure 4.** The constraints on possible orbital properties and origin of S5-HVS1, assuming that it was ejected from a point in the Galactic plane. $X_{pl}$ and $Y_{pl}$ are the Galactocentric coordinates of the ejection point in the plane. $D_{hel}$ is the current distance to the star and $V_{3D,now}$ is the current velocity of the star in the Galactocentric frame. The blue and green contours and curves refer to the posterior that we obtained while using the photometric only distance (Model P) and spectrophotometric distance (Model SP), respectively. We note that the $D_{hel}$ distributions are exactly the same as in Fig. 3, as we reuse the samples from the SED modelling posterior. The dashed lines identify the location of the GC. The lines in the contour plots show the 68 per cent, 95 per cent, and 99.7 per cent posterior volumes.

are interested in is whether the star has been ejected from the GC, the MW disc, or some other system such as a globular cluster or satellite galaxy. While some fast moving stars have been associated with other galaxies like the Large Magellanic Cloud (Edelmann et al. 2005; Gualandris & Portegies Zwart 2007; Boubert & Evans 2016; Boubert et al. 2017; Irrgang et al. 2018; Erkal et al. 2019); in this paper, we will focus only on ejection from the MW disc and the GC.

To infer a possible ejection point and velocity of S5-HVS1, we integrate the orbit of the star backwards in time in the gravitational potential of the Milky Way until the star intersects the Galactic plane $Z = 0$ at the location $X_{pl}$, $Y_{pl}$. Throughout the paper when doing orbit integrations, unless specified otherwise, we adopt the gravitational potential from McMillan (2017), the distance from the Sun to GC of 8.178 kpc (Gravity Collaboration et al. 2019), and Solar velocity of $(U_\odot, V_\odot, W_\odot) = (11.1, 245, 7.25)$ km s$^{-1}$ (Schönrich, Binney & Dehnen 2010; McMillan 2017). To take into account the observational uncertainties in our inference of the ejection site $X_{pl}$, $Y_{pl}$, when integrating back the orbit of S5-HVS1 we sample the observed uncertainties in radial velocity from $S^5$, proper motion from *Gaia* and the distance posterior derived in Section 3.3. The resulting distributions of the Galactic plane ejection coordinates $X_{pl}$, $Y_{pl}$ together with current heliocentric distance $D_{hel}$ and current velocity in the Galactocentric frame $V_{3D,now}$ are shown in Fig. 4. The two sets of distributions shown with green and blue correspond to the photometric only distance (Model P) and spectro-photometric distance (Model SP) constraints. We remark that the current heliocentric distance $D_{hel}$ distribution is exactly the same as the posterior on $D_{hel}$ determined in Section 3.3. While the figure shows the Monte Carlo sampling of uncertainties, it is mathematically equivalent to the posterior distribution of $P(X_{pl}, Y_{pl}, D_{hel}, V_{3D,now}|\text{Data})$ under the model where the star was ejected from MW disc plane (and uninformative priors on $X_{pl}$, $Y_{pl}$ and ejection velocity).

As expected, the posterior on the S5-HVS1 ejection point is very elongated (almost one dimensional) due to the negligible uncertainties in all parameters but the heliocentric distance. However, we also see that the usage of spectrophotometric distances alleviates this problem somewhat. The current total velocity of the star in the Galactic rest frame is constrained to be $V_{3D,now} = 1470^{+170}_{-150}$ km s$^{-1}$ for Model P and $V_{3D,now} = 1687^{+39}_{-37}$ km s$^{-1}$ for Model SP, while the ejection velocity of the star from the Galactic disc is $V_{ej} = 1550^{+190}_{-160}$ km s$^{-1}$ for Model P, and $V_{ej} = 1755^{+45}_{-44}$ km s$^{-1}$ for Model SP, very similar to the current velocity. The difference between the current velocities and the ejection velocities is small ($\sim$50 km s$^{-1}$) because the impact of the Galactic potential on such a fast moving star is minimal. The inferred ejection point based on the photometric only distance (Model P) is $X_{pl} = -2.63^{+1.72}_{-1.54}$ kpc, $Y_{pl} = -0.22^{+0.15}_{-0.10}$ kpc, where the values and uncertainties come from 50 per cent and 16 per cent, 84 per cent percentiles of 1D marginal distributions. However, the constraints on $X_{pl}$, $Y_{pl}$ are strongly non-Gaussian and elongated. Most importantly we see that the GC ($X$,

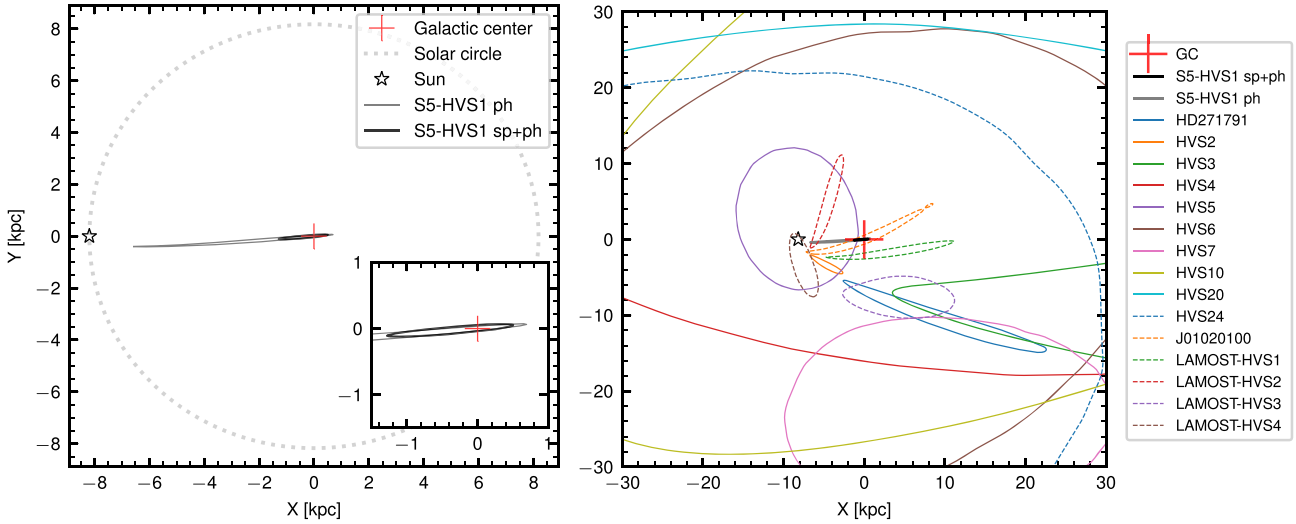


**Figure 5.** *Left-hand panel:* The constraints on the origin of S5-HVS1 in the Galactic plane. The location of the Sun, Solar circle, and the GC are indicated by a star symbol, grey dotted line, and red cross, respectively. The black contour shows the 90 per cent confidence region of the origin of S5-HVS1 constructed using spectrophotometric distances, while the grey contour shows the constraints if we use less well-determined photometric only distances. Both of these contours contain the GC. The small inset shows the central 2.5 × 2.5 kpc$^2$ region around the GC. *Right-hand panel:* 90 per cent confidence regions in Galactic $X$, $Y$ for the point of origin of various hyper-velocity stars under the assumption that they come from the Galactic plane. We only included stars with contours that significantly overlap with the 30 × 30 kpc$^2$ region shown. The confidence regions for the S5-HVS1 origin are the barely visible grey and black streaks around the GC compared to all other stars.

$Y$) = (0, 0) (shown on Fig. 4 by pink dashed lines) is located within the 90 per cent probability contour of the $X_{\rm pl}$, $Y_{\rm pl}$ distribution. While the peak of the posterior for the ejection point $X_{\rm pl}$, $Y_{\rm pl}$ is shifted by 2.5 kpc from the GC, the fact that the very thin probability contour covers the GC is highly informative and suggestive of a GC origin. If we instead consider the contours for Model SP based on spectrophotometric distances, we see that the inference of $X_{\rm pl}$, $Y_{\rm pl}$ is significantly tighter $X_{\rm pl} = -0.37^{+0.40}_{-0.39}$ kpc, $Y_{\rm pl} = -0.03^{+0.05}_{-0.04}$ kpc, and thus our backward integrations point almost unambiguously at the GC ($X_{\rm pl}$, $Y_{\rm pl}$) = (0, 0) as the origin of S5-HVS1.[10]

To further illustrate the strength of evidence supporting an association of S5-HVS1 with the GC we look at the confidence region of the S5-HVS1 origin and compare it to the Solar circle. The left-hand panel of Fig. 5 shows the 90 per cent confidence region for S5-HVS1 when relying on spectrophotometric distances (the black contour), and photometric only distances (grey contour). Both of the 90 per cent confidence limits well encompass the GC. We also see that even the less well-constrained Model P contour is extremely thin compared to the Solar circle, suggesting that it would be quite unlikely for it to cover the GC by random chance. This conclusion applies even more strongly for the minutely thin contours of Model SP as shown by the black line. To formally quantify the statistical significance of the association of S5-HVS1 with the GC, we can use the posterior on $X_{\rm pl}$, $Y_{\rm pl}$ to compute the Bayes factor (see e.g. Trotta 2007) between the hypothesis that the star comes from the GC versus that it comes from a random point in the Galactic disc. To do this, we have to adopt a prior on $X_{\rm pl}$, $Y_{\rm pl}$ for the Galactic disc origin hypothesis. We use the exponential distribution with a scale length of 2.15 kpc, to match the distribution of stellar mass in the disc (Bovy & Rix 2013). With this prior we can then use the Savage–Dickey ratio (Verdinelli & Wasserman 1995) to evaluate the Bayes factor of the two hypotheses: GC and disc.

$$K = \frac{P(\mathrm{GC}|\mathrm{Data})}{P(\mathrm{disc}|\mathrm{Data})}\frac{\pi(\mathrm{disc})}{\pi(\mathrm{GC})} = \frac{P(X_{\rm pl}, Y_{\rm pl} = 0, 0|\mathrm{disc}, \mathrm{Data})}{\pi(X_{\rm pl}, Y_{\rm pl} = 0, 0|\mathrm{disc})}.$$

The Bayes factor is $K = 81$ when we use photometric distances (Model P), and $K = 354$ for the spectrophotometric distances (Model SP). This constitutes strong (Model P) or overwhelming (Model SP) evidence in favour of the GC origin. In the calculation, we assumed the same (uniform) priors over ejection velocities, direction and traveltime in both hypotheses. An intuitive explanation of a Bayes factor of 354 is that if before observing S5-HVS1 the odds ratio in favour of the GC origin versus disc origin was 50/50, then after observing S5-HVS1 we would have to update the odds to be 354/1.

The evidence that S5-HVS1 is coming from the GC is almost definitive and is much stronger than for any other hyper-velocity star we know. To illustrate this, we take the list of stars from Boubert et al. (2018, augmented with LAMOST-HVS4 from Li et al. 2018, and J01020100 from Massey et al. 2018) and perform the calculation of the ejection point $X_{\rm pl}$, $Y_{\rm pl}$ within the plane of the disc (identically to that performed on S5-HVS1), given the existing observational constraints on those stars (position, distances, proper motions, and radial velocities). The right-hand panel of Fig. 5 shows the 90 per cent confidence contours for a subset of the stars where those contours overlapped significantly with the 30 × 30 kpc$^2$ region (for many stars in the list, e.g. HVS1, the contours are larger than the whole plot). The figure shows that there are stars that could be associated with the GC based on their phase space coordinates (for instance, HVS20 and HVS24), but their confidence region of origin includes the whole Milky Way disc as well. Among other stars with tighter constraints on the point of origin, only J01020100 (Massey et al. 2018) seems to cover the

[10]While the backward orbit integration done here uses the potential of McMillan (2017), which does not include the SMBH in the GC, we have verified that the constraints on the ejection point ($X_{\rm pl}$, $Y_{\rm pl}$) are completely insensitive to the presence or absence of a ∼4 × 10$^6$ M$_\odot$ BH in the GC due to its very small sphere of influence compared to the size of the ($X_{\rm pl}$, $Y_{\rm pl}$) contours.

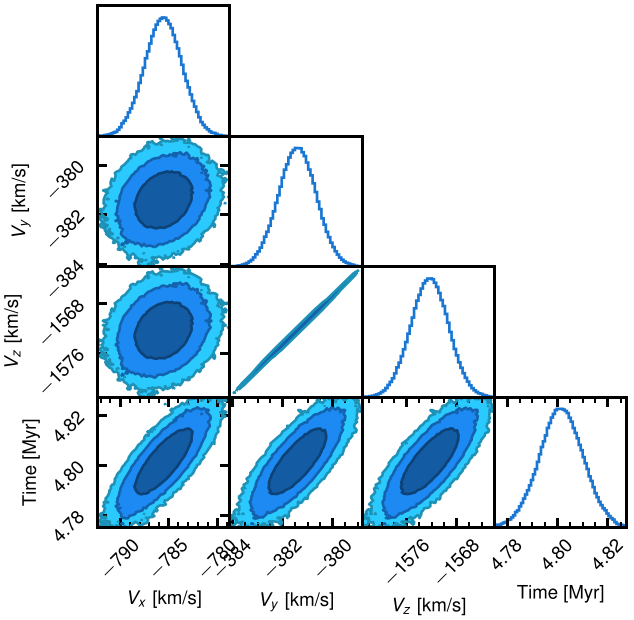


**Figure 6.** The constraints on the 3 Galactic components of the ejection velocity and traveltime to the current location of S5-HVS1, assuming a GC origin. The total ejection velocity is ∼1800 km s$^{-1}$ oriented downwards from the Galactic plane and somewhat towards the Sun.

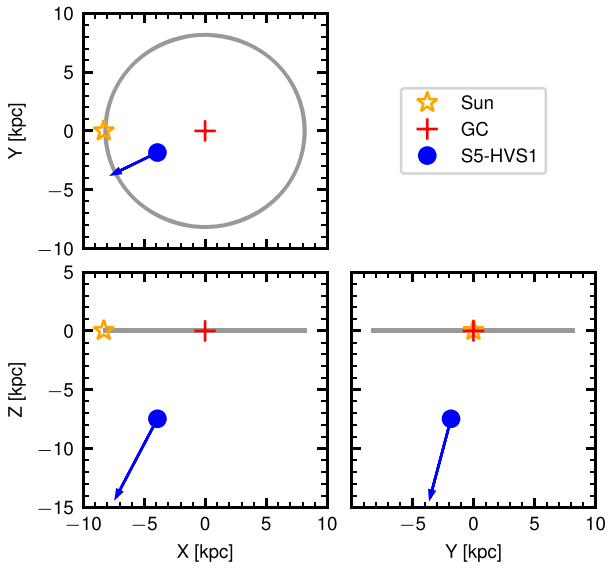


**Figure 7.** The location and direction of motion of S5-HVS1 in the Galaxy assuming a GC origin. Three panels show different projections in Galactic Cartesian coordinates. The location of the Sun, the GC, and the Solar circle are marked by the orange star, red cross, and grey circle, respectively. The arrow shows the direction of S5-HVS1's velocity in the corresponding projection. The length of the arrow corresponds to the distance travelled by the star in 4 Myr.

GC (but note that J01020100 is believed to be a disc runaway due its meagre velocity of 296 km s$^{-1}$). The contour showing the region of origin of S5-HVS1 around the GC is almost invisible compared to the other stars.

Concluding this section, based on strong orbital evidence that points at a region of ∼50 × 1000 pc$^2$ around the GC as the origin of S5-HVS1 (Fig. 5) and the large velocity of S5-HVS1 $V_{3D,now}$ ∼ 1500–1700 km s$^{-1}$ that is impossible for a disc runaway star of ∼2 M$_\odot$ (see Tauris 2015), we can conclude that S5-HVS1 was ejected from the GC. It is the first star with such a confident identification. In the next section, we will analyse what inferences can made based on this assumption.

## 5 GC ORIGIN

Assuming that S5-HVS1 was ejected from the GC, we can now investigate the kinematics of the star further. First, we determine the exact ejection velocity and time of flight from the GC required to match the observations of S5-HVS1, by ejecting the star from the centre of the MW in the potential of McMillan (2017) (without considering the potential of the SMBH itself). This gives a prediction of $\alpha$, $\delta$, $\mu_\alpha$, $\mu_\delta$, $RV$, $D_{\rm hel}$ as a function of the ejection velocities $V_x$, $V_y$, $V_z$, and traveltime $T$. We then write a Normal likelihood function using the observed position, distance, proper motion, and RV of S5-HVS1 and their uncertainties (we use a Gaussian approximation to the $\log_{10}D_{\rm hel}$ posterior from Section 3.3). We adopt non-informative uniform priors on all the parameters and then sample the posterior using an ensemble sampler. Fig. 6 shows the posterior. This model implies an ejection speed of 1798.6 ± 3.1 km s$^{-1}$ with the $z$-component of the velocity being the largest and a total traveltime from the GC to the current position of 4.801 ± 0.009 Myr. We note that the constraints on the ejection velocities are now much tighter compared to Fig. 4. The reason for this is that postulating that the star is coming from the GC strongly constrains the current distance to S5-HVS1 to be $D_{\rm hel}$ = 8884 ± 11 pc and thus makes our spectro-photometric measurement mostly irrelevant.[11] We also remark that the measured ejection speed of 1798.6 ± 3.1 km s$^{-1}$ from the GC was computed while ignoring the potential of the SMBH, and thus represents the ejection velocity outside the sphere of influence of the black hole ($\gtrsim$1 pc). The actual ejection speed of the star depends on how close to the BH the ejection happened, and could easily be as high as ∼8000 km s$^{-1}$ if the ejection happened at a distance of 100 au from the BH. Assuming a GC origin also allows us to improve the proper motion precision from the one delivered by *Gaia* $\mu_\alpha \cos\delta = 35.333 \pm 0.081$ mas yr$^{-1}$ and $\mu_\delta = 0.617 \pm 0.011$ mas yr$^{-1}$. While the $\mu_\alpha \cos\delta$ precision did not improve much, the error bar on the predicted $\mu_\delta$ is 8 times smaller than *Gaia*'s. Since the full phase space position of S5-HVS1 becomes very precise when we adopt the GC origin hypothesis, we can look at the geometric position of S5-HVS1 in the Galaxy. This is shown in Fig. 7. We see that, as expected, S5-HVS1 is mostly moving downwards away from the disc and that the Sun, GC, and S5-HVS1 form an almost equilateral triangle with ∼8–9 kpc edges.

In this section, we will further use the phase space observations of S5-HVS1 to constrain the gravitational potential of the MW, location, and kinematics of the Sun in the Galaxy, and assess the possible connection of S5-HVS1 to the stars in the vicinity of Sgr A*.

### 5.1 Constraining the position and motion of the Sun

Fig. 5 shows that the association of S5-HVS1 with the GC crucially depends on the relative geometry between the Sun and the GC. For example, a small adjustment of the distance from the Sun to the

[11] Given a star ejected from the GC, it is enough to know accurately just the position of the star on the sky and proper motion to exactly determine its heliocentric distance and radial velocity.

GC ($R_0$) could easily shift the high probability contour $\mathcal{P}(X_{\rm pl}, Y_{\rm pl})$ away from the GC. Therefore, assuming that S5-HVS1 originates in the GC constrains $R_0$ and possibly other Galactic parameters. The idea of constraining the Solar motion as well as the distances to the GC have been discussed previously, most notably by Hattori et al. (2018b). To determine these constraints, we construct a forward model where we eject the star from the GC with velocity $V_x$, $V_y$, $V_z$, and let it travel in the Galactic potential of McMillan (2017) for the time $T$. We then observe it from the Sun located at a distance of $R_0$ from the GC and moving with the velocity $\mathrm{U}_\odot$, $\mathrm{V}_\odot$, $\mathrm{W}_\odot$ km s$^{-1}$ (this includes both the speed of the Local Standard of Rest and the peculiar velocity of the Sun). The likelihood of the model is then constructed using the observed 6D phase measurements of S5-HVS1: position, proper motion, distance, and radial velocity. This leads to the following posterior distribution:

$$\mathcal{P}(\psi|D) \propto \mathcal{P}(D|V_x, V_y, V_z, T, \mathrm{R}_0, \mathrm{U}_\odot, \mathrm{V}_\odot, \mathrm{W}_\odot) \\ \pi(V_x, V_y, V_z)\pi(R_0)\pi(\mathrm{U}_\odot, \mathrm{V}_\odot, \mathrm{W}_\odot)\pi(T), \quad (2)$$

where $\psi$ is the shorthand for all the model parameters $V_x$, $V_y$, $V_z$, $T$, $R_0$, $\mathrm{U}_\odot$, $\mathrm{V}_\odot$, $\mathrm{W}_\odot$. For this model, we focus on constraining $R_0$ and $\mathrm{V}_\odot$, so we adopt broad uninformative priors on the distance of the Sun to the GC $\frac{R_0}{1\,\mathrm{kpc}} \sim \mathcal{U}(6, 9)$, and $\frac{\mathrm{V}_\odot}{1\ \mathrm{km\,s^{-1}}} \sim \mathcal{U}(200, 290)$ and informed Normal priors on the other two components of Solar velocity $\frac{\mathrm{U}_\odot}{1\ \mathrm{km\,s^{-1}}} \sim \mathcal{N}(11.1, 0.5)$, $\frac{\mathrm{W}_\odot}{1\ \mathrm{km\,s^{-1}}} \sim \mathcal{N}(7.25, 0.5)$ (Schönrich et al. 2010). For the rest of parameters $V_x$, $V_y$, $V_z$, $T$ we adopt uninformative uniform priors. In principle the model that we have described has a valid posterior that we could sample. However, we have discovered that this posterior is extremely degenerate along one dimension and narrow in another dimension. This is in fact a direct consequence of the elongated contour shape for the constraint on the ejection point $X_{\rm pl}$, $Y_{\rm pl}$ seen in Fig. 5. This contour shape and the fact that simultaneous changes of $\mathrm{V}_\odot$ and $R_0$ give two degrees of freedom for 'moving' the high probability contour in $(X_{\rm pl}, Y_{\rm pl})$ space while still covering the GC explains the long degeneracy ridge in the posterior. Furthermore, the posterior is also extremely narrow along the time axis, as the orbit needs to pass very close to the precisely known observed position on the sky. It turns out that those features of the posterior make it extremely challenging to sample, so we were unable to do it efficiently using either MULTINEST, DYNESTY, ensemble or ensemble parallel tempering samplers (EMCEE). Our solution to this problem was to adopt an approximation to the posterior where we approximately marginalize over the traveltime of the star:

$$\mathcal{P}(\psi|D) \propto \mathcal{P}(D|V_x, V_y, V_z, T_{\rm max}, \mathrm{R}_0, \mathrm{U}_\odot, \mathrm{V}_\odot, \mathrm{W}_\odot) \\ \pi(V_x, V_y, V_z)\pi(R_0)\pi(\mathrm{U}_\odot, \mathrm{V}_\odot, \mathrm{W}_\odot), \quad (3)$$

where $\psi$ is the shorthand for the model parameters $V_x$, $V_y$, $V_z$, $R_0$, $\mathrm{U}_\odot$, $\mathrm{V}_\odot$, $\mathrm{W}_\odot$, and

$$T_{\rm max} = \arg\max_{\rm T} \mathcal{P}(D|V_x, V_y, V_z, T, R_0, \mathrm{U}_\odot, \mathrm{V}_\odot, \mathrm{W}_\odot).$$

Thus, $T_{\rm max}$ is the traveltime that maximizes the likelihood (or approaches the current phase-space constraint of S5-HVS1 the most closely). We find the $T_{\rm max}$ for each set of parameters by doing 1D maximization using the Brent algorithm (Brent 2013). The resulting posterior on $V_x$, $V_y$, $V_z$, $R_0$, $\mathrm{U}_\odot$, $\mathrm{V}_\odot$, $\mathrm{W}_\odot$ is then sampled using an ensemble sampler with 192 walkers.

The left-hand panel of Fig. 8 shows the 2D marginalized posterior on two of the parameters – heliocentric distance to the GC and the Y component of the Solar velocity ($\mathrm{V}_\odot$). As before blue lines correspond to Model P (photometric only distance), and green lines to Model SP (spectrophotometric distance). The red bands show

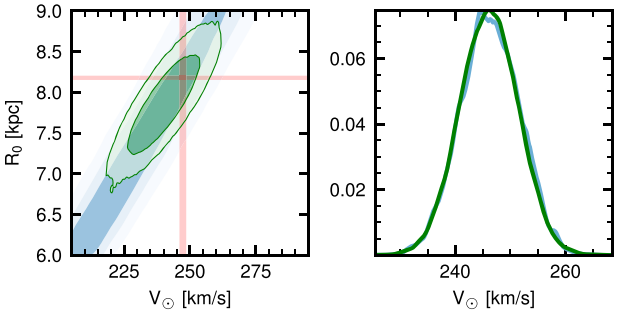


**Figure 8.** *Left-hand panel*: The 2D marginalized posteriors on the heliocentric distance to the GC ($R_0$) and $y$-component of Solar velocity in the Galaxy as inferred from S5-HVS1. The contours correspond to the 68 per cent and 95 per cent posterior volumes. Blue lines on both panels refer to quantities derived from our photometric only distance (Model P), while the green ones refer to the more precise spectrophotometric distances (Model SP). The red bands show the constraints on $R_0$ and $\mathrm{V}_\odot$ from Gravity Collaboration et al. (2019). *Right-hand panel:* 1D marginal posteriors on the $y$-component of Solar velocity in the Galactic rest frame after adopting a prior on $R_0$ from Gravity Collaboration et al. (2019). The inferred value is $\mathrm{V}_\odot = 246.1 \pm 5.3$ km s$^{-1}$.

the $1\sigma$ constraints from Gravity Collaboration et al. (2019). As expected the figure shows a degeneracy between parameters that is almost complete when using the less constrained photometric only distances; however, with spectrophotometric distances the degeneracy is significantly reduced.

We note that even with the spectrophotometric distances of S5-HVS1 we cannot strongly constrain both $\mathrm{V}_\odot$ and $R_0$ (as the green contours on Fig. 8 are quite large). However, if we adopt the prior on the Galactocentric distance from Gravity Collaboration et al. (2019), we obtain the posterior on $\mathrm{V}_\odot$ shown on the right-hand panel of the figure. $\mathrm{V}_\odot$ is constrained to be $246.1 \pm 5.3$ km s$^{-1}$. Those constraints also do not depend significantly on whether we use spectrophotometric or photometric only distances as we slice the posterior shown on the left-hand panel of the figure across the distance degeneracy. The $\mathrm{V}_\odot$ measurement is competitive with and entirely independent from the $247.4 \pm 1.4$ km s$^{-1}$ constraint from Gravity Collaboration et al. (2019). If we instead use the prior on $\mathrm{V}_\odot$ from Gravity Collaboration et al. (2019) to constrain the distance to the GC (marginalizing over the $x$-axis on Fig. 8), we obtain $R_0 = 8.12 \pm 0.23$ kpc.

While Fig. 8 may look somewhat underwhelming compared to the Gravity Collaboration et al. (2019) measurements, we highlight that our measurement was done with one single star. The shape of the degeneracy in $\mathrm{U}_\odot$, $\mathrm{V}_\odot$, $\mathrm{W}_\odot$, $R_0$ space is specific to the position of the star on the sky, and so if we had a second star then the combined constraints would be significantly more precise and likely comparable in precision to Gravity Collaboration et al. (2019).[12] Another reason for optimism is that future *Gaia* data releases and high-resolution spectroscopic follow-up will narrow the uncertainties on the proper motion and distance of S5-HVS1 and thus tighten our constraints on the Solar motion and position in the Galaxy.

[12]In fact in this paper we did not consider determining $\mathrm{U}_\odot$, $\mathrm{W}_\odot$, because they are significantly less constrained than $\mathrm{V}_\odot$. That can be easily seen because of the shape of the contour of $\mathcal{P}(X_{\rm pl}, Y_{\rm pl})$ on Fig. 5. The contour is the thinnest in the direction of solar rotation and is larger by a factor of 10 in the $U$ direction.

### 5.2 Constraints on the Galactic potential

As we showed in the previous section, S5-HVS1 strongly constrains the Galactic position and velocity of the Sun. On top of that we expect that – under the assumption that the star comes from the GC – the observed properties of the star should also constrain the gravitational potential of the MW. This idea was first proposed by Gnedin et al. (2005), who suggested using individual HVS with accurate phase-space positions to measure the MW Dark Matter (DM) halo flattening. This idea has been extended to the modelling of the HVS population as a whole as it is being deflected by the disc and flattened MW halo away from an initial distribution over angles (Yu & Madau 2007; Contigiani, Rossi & Marchetti 2019).

It turns out, however, that while the proximity of S5-HVS1 was essential for precise measurements of its properties and its detection, the short flight time of ∼5 Myr from the GC makes the orbit of the star barely sensitive to the MW potential. To gain an intuition for this, it is useful to look at the inferred position where the star crosses the MW plane $\mathcal{P}(X_{\rm pl}, Y_{\rm pl})$ in Figs 4 and 5, when we were backtracking the current phase-space coordinates to the Galactic plane. The reason why the potential could be constrained by the S5-HVS1 is because when we change the gravitational potential, the distribution of $X_{\rm pl}$, $Y_{\rm pl}$ changes, and high probability contours are shifted away from $(X_{\rm pl}, Y_{\rm pl}) = (0, 0)$ making such potentials less likely under the hypothesis that the GC is the origin of the S5-HVS1. However even if we turn-off the MW potential completely, the offset in the point of the Galactic plane crossing $X_{\rm pl}$, $Y_{\rm pl}$ for orbits that backtrack from the current phase space position of the star to approximately the GC is a mere ∼15 pc, which is less than the width of the distribution $X_{\rm pl}$, $Y_{\rm pl}$. Similarly, setting the MW disc mass to zero causes a shift in $X_{\rm pl}$, $Y_{\rm pl}$ of ∼13 pc. If we take the potential of McMillan (2017) and vary the flattening (in density) of the Navarro–Frenk–White (Navarro, Frenk & White 1997) DM halo from default $q_{\rm DM,halo} = 1$ to 0.5 or 2 that results in offsets of only ∼7 and 18 pc respectively.

This lack of sensitivity to the DM halo flattening was confirmed when we obtained the formal posterior on $\mathcal{P}(q_{\rm DM,halo}|D)$ under the hypothesis of ejection from the GC and found that it was consistent with the prior. This shows that with the current proper motion precision, S5-HVS1 cannot yet be used to constrain the MW gravitational potential. One additional reason for the current lack of constraining power from S5-HVS1 is that, because we do not know the actual ejection velocity from the BH, we do not constrain the total deceleration of the star, but only deviations of the trajectory from a straight line. For meaningful potentials consistent with the existing data, the deviations from a straight line for a ∼2000 km s$^{-1}$ star flying for ∼5 Myr are within a few tens of parsecs (listed above) and thus within the current uncertainties of the S5-HVS1 trajectory. With the improvement in proper motion precision from future *Gaia* data we expect, however, that constraints on the MW halo flattening will be possible.

### 5.3 S5-HVS1 ejection by Sgr A*

Given an almost certain GC origin of S5-HVS1, here we discuss possible implications for the ejection by Sgr A*. We focus on the Hills (1988) mechanism involving a three-body interaction of a stellar binary with the SMBH, leading to one star being ejected. There are other mechanisms involving binary black holes (Yu & Tremaine 2003; Levin 2006) and an SMBH surrounded by a cluster of stellar mass black holes (O'Leary & Loeb 2008), and we will discuss some of them later.

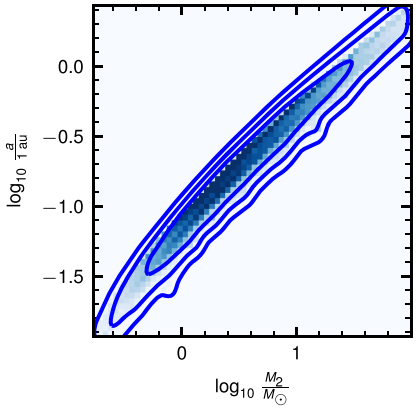


**Figure 9.** The distribution of semimajor axis of the binary system and mass of a secondary that could have produced S5-HVS1 via the Hills mechanism. The contours encircle the 68 per cent, 95 per cent, and 99.7 per cent posterior volumes.

The first question we address is what are the expected properties of the binary required to produce the very high ejection speed of S5-HVS1. To infer this we use the results of Bromley et al. (2006), who parametrized the distribution of ejection velocities as a function of the black hole mass and binary parameters (see equations 1–4 of Bromley et al. 2006). We adopt a black hole mass of $4.1 \times 10^6\,{\rm M}_\odot$ from Gravity Collaboration et al. (2018), fix the mass of S5-HVS1 to the observed value $2.35\,{\rm M}_\odot$ (see Table 2) and adopt an ejection velocity of $1798 \pm 3$ km s$^{-1}$. The remaining parameters required to compute the ejection velocity distribution are the semimajor axis of the binary $a$, the mass of the second star $M_2$, and the minimum approach distance $R_{\rm min}$ between the binary and the SMBH. We adopt a log-uniform distribution over the binary separation and the Chabrier (2005) IMF prior on the mass of the secondary, and $\pi(R_{\rm min}) \sim R_{\rm min}$ prior for the minimum approach distance (see Bromley et al. 2006 for details). We require that the semimajor axis of the binary is larger than $2.5{\rm R}_\odot$, which is approximately the expected radius of a star with a mass of $\sim 2.35\,{\rm M}_\odot$ (Boyajian et al. 2013), and that the radius of S5-HVS1 is smaller than its tidal radius at the closest approach between the binary and the SMBH ($R_{\rm min}$). This limits the minimal separation of the binary and the SMBH $R_{\rm min}$ to be $\gtrsim$1.4 au.

Fig. 9 shows our inferred probability distribution of the semimajor axis of the binary and mass of the second star. The distribution shows that in order to produce S5-HVS1 we need a former binary companion with mass $0.9\,{\rm M}_\odot \lesssim M_2 \lesssim 16\,{\rm M}_\odot$, where low-mass secondaries require an extremely tight separation of only ∼0.06 au, while if the secondary is massive, the semi-major can be as much as ∼0.63 au. The orbital periods of these binaries would range from 3 to 40 d. These ranges correspond to the 68 per cent confidence interval of the posterior. The binary parameters that we obtain are certainly possible (see e.g. Raghavan et al. 2010; Moe & Di Stefano 2013); however, we expect these binaries to be quite rare.

### 5.4 S5-HVS1 and stars around Sgr A*

Given the certainty of the S5-HVS1 association with the GC, it is interesting to assess if S5-HVS1 is related to any other structures known around the GC. The main stellar structure near the centre of the MW is the nuclear star cluster (Becklin & Neugebauer 1968; Launhardt, Zylka & Mezger 2002) with the Sgr A* SMBH at the centre. The central part of the star cluster consists of the so-called S-stars whose dynamics are dominated by the SMBH and that orbit

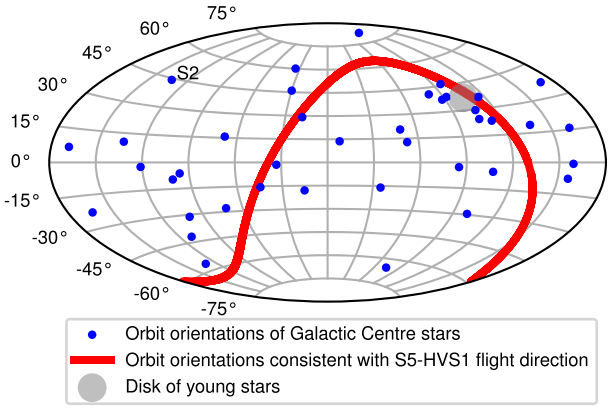


**Figure 10.** The orientation of orbital planes of stars around the GC compared to the possible orbital plane of the binary system around the GC that S5-HVS1 was member of. The coordinate system of the figure is the positional angle of ascending node of the orbit versus inclination of the orbit with respect to the line of sight. Blue circles identify orbits of stars from Gillessen et al. (2017), while the red curve shows a set of possible planes consistent with S5-HVS1. The red curve also identifies the potential orbital plane of the secondary star of S5-HVS1 binary if it still orbits the SMBH and if S5-HVS1 was ejected by Hills mechanism. The grey circle marks the overdensity of stars on an orbital plane associated with the disc of young stars (Bartko et al. 2009; Yelda et al. 2014).

around it with periods from a few years to a few hundred years (Ghez et al. 2005; Gillessen et al. 2009). These stars are known to be massive and young (Genzel, Eisenhauer & Gillessen 2010; Lu et al. 2013) and we do not yet know how they came to be where they are. Furthermore, the cluster of stars around Sgr A* is known to have substructure in the form of a coherently rotating small disc of young stars (the so-called clock-wise or CW disc) (Levin & Beloborodov 2003; Paumard et al. 2006; Bartko et al. 2009; Yelda et al. 2014; Gillessen et al. 2017).

The reason why S5-HVS1 can be potentially associated to some structures in the centre is that if the star has been produced by the Hills mechanism, then we expect that the direction of HVS's flight should be approximately aligned (Lu, Zhang & Yu 2010; Zhang, Lu & Yu 2010) with (i) the orbital plane of the original binary around the SMBH; and (ii) the orbital plane of the secondary star captured by the SMBH after the binary disruption (unless the secondary was swallowed by the black hole and/or produced a tidal disruption event). Thus, we can hope to either identify a possible progenitor population of the S5-HVS1 binary or perhaps directly pinpoint the star that was previously paired to S5-HVS1 and still orbits Sgr A*.

To check for possible association with the S-stars, we consider a set of possible orbital planes around the black hole that are aligned with the S5-HVS1 direction of flight. This set is clearly a 1D manifold, as there are infinitely many planes aligned with the vector pointing from the GC to S5-HVS1. In Fig. 10, we show the distribution of poles (or angular momentum directions) for this set of orbits by a red curve. The coordinate system of the figure is the positional angle of the ascending node of the orbit and the angle between the orbital plane with respect to the vector from the Sun to the GC. Therefore, the orbits seen edge-on from the Sun would occupy the equator on the figure, while face-on orbits would correspond to either the north or the south pole of the figure depending on the direction of rotation. In this figure, we also overplot by blue circles the orientations of orbits (specifically the direction of their angular momenta) for stars around Sgr A* from Gillessen et al. (2017). Thus if the S5-HVS1 has been produced by the Hills mechanism and the secondary star was captured on an orbit around the BH, then the red curve should pass near the current orbital plane of the secondary star. In this figure, we also mark by a grey circle the concentration of orbital poles corresponding to the disc of young stars observed around the GC (Bartko et al. 2009; Yelda et al. 2014). We see that the red line comes close to many S stars, which is not surprising and is expected to happen by chance. However, we see that the red curve also crosses the concentration of blue points marked by the grey circle, meaning that S5-HVS1 flies within the orbital plane of young stars around the GC. This is potentially very interesting, because it may mean that the binary responsible for S5-HVS1 has the same origin as the young stellar disc. Several formation scenarios for it exist, that either involve the infall of a gas cloud on the GC with subsequent star formation (Bonnell & Rice 2008), or star formation in the disc around the SMBH (Nayakshin, Cuadra & Springel 2007). This disc could then potentially be the source of the S5-HVS1 binary (i.e. due to orbit instabilities discovered by Madigan, Levin & Hopman 2009) and S5-HVS1 would provide us with an opportunity of studying the stars in disc without all the complexities of observing through tens of magnitudes of extinction. In this scenario, the secondary of the S5-HVS1 could still be in the disc and thus could be potentially identified.

Alternatively, the young disc may consist of captured secondary stars from binaries disrupted in the Hills mechanism, in which case the previous partner of S5-HVS1 may be still in that disc. We note, however, that the young stellar age of the stars in the disc of a few Myr (Lu et al. 2013), and the low eccentricities of stars in the disc (Yelda et al. 2014) make this scenario unlikely because the captured stars in Hills mechanism are expected to have high eccentricities (Hills 1988).

## 6 DISCUSSION

Here we address the multiple open questions that the discovery of S5-HVS1 poses. First, we compare S5-HVS1 to the other HVS. The main property that distinguishes S5-HVS1 from the rest of the hyper-velocity stars is its unusually high velocity. If we exclude the recently discovered D$^6$ WDs produced in SNIa-like explosions (Shen et al. 2018), the velocity of S5-HVS1 is almost a factor of two larger than the velocity of any other known HVS. Fig. 11 shows the distribution of likely ejection velocities from the GC for other HVS. Here we use the same set of stars from Boubert et al. (2018) as shown on Fig. 5, and select a subset of those which can be well described ($\chi^2 < 20$) as being ejected from the GC based on proper motion, position, distance and radial velocity. The figure shows how much of an outlier S5-HVS1 is, in particular because of the apparent clumping of previously known HVS at 800–1000 km s$^{-1}$, which begs the question whether S5-HVS1 was produced using the same mechanism as other HVS. Another difference between S5-HVS1 and other HVS is that it is an A-type star, and thus is somewhat cooler, lower mass and later spectral type than the classical B-type hyper-velocity stars (Brown 2015). It is also brighter and much more nearby than the majority of the faint, blue HVS that have been discovered in the Northern sky.

One possible interpretation of these differences between S5-HVS1 and previously known HVS is that S$^5$ was just very lucky to stumble on a very rare object. However, the other explanation may be related to the somewhat lower mass and redder colour of S5-HVS1 $g - r = -0.27$, which is close to the colour boundary $g - r \sim -0.3$ of dedicated searches (Brown et al. 2006; Brown,

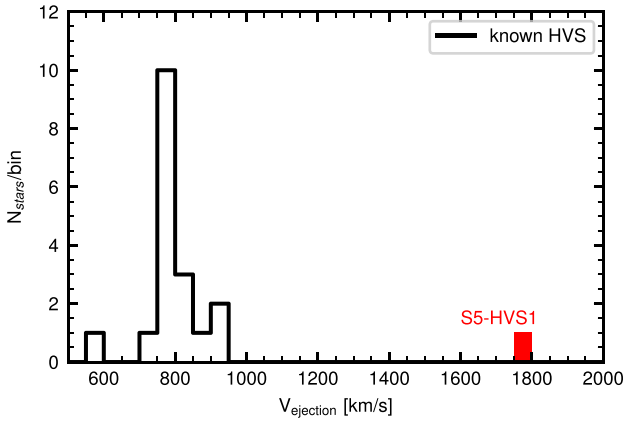


**Figure 11.** The distribution of possible ejection velocities from the GC computed for the subset of known HVS from Boubert et al. (2018) whose phase-space measurements (position, velocities, proper motions and distance) are consistent with a GC ejection. S5-HVS1 is highlighted in red.

Geller & Kenyon 2009); this boundary minimizes contamination because MS and BHB stars start to overlap at this colour. This may be the reason why previous spectroscopic searches missed lower mass/redder stars like S5-HVS1. However, since the Sloan Digital Sky Survey (SDSS; York et al. 2000; Yanny et al. 2009) did observe a large number of blue A-type stars in the range $-0.4 < g - r < 0$ and did not find anything close to S5-HVS1, it is useful to compare the number of objects spectroscopically observed by SDSS to S$^5$. In fact, surprisingly, SDSS (DR9; Ahn et al. 2012) has observed spectroscopically only ∼7 times more blue, distant (with small parallax $\pi < 3\sigma_\pi$) stars in the $-0.4 < g - r < -0.2$ and $16 < g < 18$ colour–magnitude range than S$^5$ did (1445 versus 202). Thus, the SDSS non-detection of an S5-HVS1-like star is not in significant disagreement with the S$^5$ discovery.

Another possible explanation of the S5-HVS1 discovery has to do with its proximity, as the star is closer by a factor of several compared to other HVS. Why would closer HVSs be potentially noticeably faster or have a different velocity distribution? For this to happen it would require that the ejection mechanism of HVS is not operating at a constant rate and/or does not eject the same spectrum of HVS over time. In the canonical Hills (1988) mechanism where the loss cone of the SMBH is populated by slow scattering processes, such rapid changes would be problematic. However, as the presence of young (only few Myr old) stars and substructures near the GC indicate, the GC has had a very active recent history; e.g. it is likely that the GC had an accretion event of a giant molecular cloud a few Myr ago that formed new stars (Bonnell & Rice 2008; Lucas et al. 2013) that were then distributed in a disc around the SMBH. If that is the case, that accretion event could have been a source of binaries for the Hills mechanism, producing an excess of stars in the orbital plane of accretion and an increased rate of HVS ejections a few Myr ago. In such a scenario, HVSs like S5-HVS1 could serve as timers and indicators of orientation of large accretion events happening near the GC. To test this hypothesis we will, however, need to find more stars with similar travel times as S5-HVS1. It is remarkable that the age of S5-HVS1 ejection is close to both the age of the disc of young stars around the GC (Lu et al. 2013) and the age of the Fermi bubbles (Bland-Hawthorn & Cohen 2003; Su, Slatyer & Finkbeiner 2010) which have been potentially associated with the recent accretion event in the GC (Zubovas, King & Nayakshin 2011; Guo & Mathews 2012), thus potentially linking these different astrophysical objects.

An alternative scenario that would naturally produce a time-variable HVS spectrum is that involving an Intermediate Mass Black Hole (IMBH) orbiting the GC (Yu & Tremaine 2003; Levin 2006). In this mechanism, during the inspiral of the IMBH, the HVS production rate peaks and then subsides due to dynamical friction around the SMBH (Baumgardt, Gualandris & Portegies Zwart 2006; Darbha et al. 2019), with the fastest HVS being ejected in the final phase of the in-spiral. This mechanism produces a strongly anisotropic distribution with the fastest stars in the orbital plane of the IMBH (Rasskazov et al. 2019). There is also some indication that the HVSs produced by this mechanism tend to have higher velocities and a flatter velocity spectrum than the classical Hills mechanism (Sesana, Haardt & Madau 2007). While there is currently not much evidence for the presence of an IMBH in the GC (Gualandris & Merritt 2009) other than a shallow stellar density slope that can be produced by an IMBH scattering (Baumgardt et al. 2006), if an IMBH inspiral happened a few Myr ago, then it would produce an excess of nearby and fast HVSs with a narrow range of ejection times. To test for this possibility we need to search for other nearby HVS and see if there is an excess of stars that were ejected at roughly the same time as S5-HVS1 (∼5 Myr ago), are strongly anisotropic and that have a velocity spectrum inconsistent with the Hills mechanism.

An interesting consequence of the fact that S5-HVS1 has lower mass than most other HVS in the halo is that its expected lifetime given the stellar mass of ∼2.3 $M_\odot$ is quite long – around a 1 Gyr. By the end of its life the star would have travelled a distance of ∼2 Mpc, traversing a large fraction of the Local Group. This suggests that searching for such ejected stars at large distances from the MW or Andromeda (Sherwin, Loeb & O'Leary 2008) is quite promising. On top of being well separated in colour–magnitude space from other contaminants, an S5-HVS1-like star would eventually evolve on to the red giant branch and thus be detectable much more easily. Searches for S5-HVS1-like stars within the whole Local Group will be possible with upcoming deep imaging surveys like LSST (LSST Science Collaboration et al. 2009).

In this paper, we tried to use the position–velocity information on S5-HVS1 to constrain the distance from the Sun to the GC and the Galactic Solar velocity. We have not been able to constrain those simultaneously, mainly due to the precision of the distance determination to S5-HVS1. However, in the future, the combination of such constraints from multiple S5-HVS1-like stars (see Fig. 8) will resolve the existing degeneracies and should provide extremely precise measurements of the geometric and kinematic Galactic parameters. We believe that with the upcoming *Gaia* DR3 as well as future spectroscopic surveys like WEAVE (Dalton et al. 2014), 4MOST (de Jong et al. 2014), and DESI (DESI Collaboration et al. 2016), the discovery of more HVS similar to S5-HVS1 is guaranteed. Furthermore, while with S5-HVS1 we were currently not able to put constraints on the gravitational potential due to the very short flight time and loose proper motion constraint, with the next *Gaia* data release that will increase the proper motion precision by a factor of few as well as deliver new HVSs, we think we will be able to start constraining the potential with individual HVS as predicted by Gnedin et al. (2005).

One other interesting prospect for the future of HVS science that we did not explore in this paper, but which may be promising, is that HVS could become probes of substructure and particularly DM substructure in the Galaxy, similar to stellar streams (Yoon, Johnston & Hogg 2011; Erkal et al. 2016) or lensing (Vegetti et al. 2012).

The reason for this is that for HVS that were ejected from the GC we know the orbit exactly, as it must connect to the GC. Thus if we imagine a large collection of HVS travelling throughout the Galaxy, we expect that some of those trajectories will be affected by various external perturbations, including massive perturbers such as the Large Magellanic Cloud or Sagittarius Dwarf Spheroidal Galaxy, but also potentially smaller DM haloes and globular clusters in the halo. Although we expect the effect of these perturbations to be quite small due the high velocity of the stars, if we have enough of these stars and they have high accuracy phase-space measurements, then we could say something about the mass substructure in the Galaxy. As an example, a $10^8$ $M_\odot$ point-mass perturbing a hyper-velocity star travelling at 2000 $km\,s^{-1}$ with an impact parameter of 0.5 kpc will produce a velocity offset of $\sim$1 $km\,s^{-1}$ (Binney & Tremaine 2011) perpendicular to the trajectory of the HVS, or equivalently an offset of $\sim$ a few parsecs in the trajectory. While these offsets are small, the velocity accuracy is within what *Gaia* proper motions will provide for objects brighter than $G \sim 17$ within 10 kpc.

Finally, let us consider the effect of future *Gaia* data releases on S5-HVS1. The main improvement will come from much higher precision parallax and proper motions, which are expected to better constrain the orbit of S5-HVS1. In advance of *Gaia* DR3, we predict that the true proper motions and parallax of S5-HVS1 are $\mu_\alpha \cos\delta = 35.333 \pm 0.080$ mas $yr^{-1}$, $\mu_\delta = 0.617 \pm 0.011$ mas $yr^{-1}$, and $\pi = 0.11$ mas (corresponding to a distance of 8.828 kpc). Time will tell whether these predictions based on the assumption of a GC origin will hold.

## 7 CONCLUSIONS

(i) Using data from the $S^5$ spectroscopic survey we have identified a star with a radial velocity of $\sim$1020 $km\,s^{-1}$ without any signs of binarity across a year of observations.

(ii) Analysis of the spectra and photometry of the star shows that it is likely an A-type $\sim$2.35 $M_\odot$ main- sequence metal-rich star at a distance of $\sim$9 kpc.

(iii) Given the measured distance, proper motion and radial velocity, the total velocity of the star in the Galactic rest frame is $1755^{+55}_{-45}$ $km\,s^{-1}$, making it the third fastest hyper-velocity (unbound) star in the Galaxy after the $D^6$ WDs (Shen et al. 2018).

(iv) Backtracking the current phase-space position of S5-HVS1 to the MW disc points at a small elongated region of $\sim 50 \times 1000$ $pc^2$ that contains the GC. This provides incredibly strong evidence that the star was ejected from the GC at speed of $\sim$1800 $km\,s^{-1}$ around $\sim$4.8 Myr ago.

(v) If S5-HVS1 was ejected from the GC then we can constrain the distance to the GC and the Solar velocity. If we assume the Gravity Collaboration et al. (2019) prior on $R_0$, then our constraint on the $y$-component of solar velocity is $V_\odot = 246.1 \pm 5.3$ $km\,s^{-1}$, and, vice versa, if the Gravity Collaboration et al. (2019) prior is used on $V_\odot$, it leads to an $R_0$ constraint of $8.12 \pm 0.23$ kpc. Due to the short flight time and non-negligible proper motion uncertainties, the star currently cannot yet constrain the MW gravitational potential.

(vi) The direction of the S5-HVS1 ejection is curiously aligned with the disc of young stars around the Sgr $A^*$, suggesting a possible connection. This may mean that the star has been ejected in the same event that leads to the disc's formation.

(vii) The fact that S5-HVS1 was ejected with a velocity almost twice that of all other known HVS potentially originating from the GC poses two questions: were all the known HVS produced by the same mechanism and has the HVS velocity spectrum been constant in time?

## ACKNOWLEDGEMENTS

This paper includes data gathered with AAT in Australia under programme A/2018B/09. We acknowledge the traditional owners of the land on which the AAT stands, the Gamilaraay people, and pay our respects to elders past and present.

This work has made use of data from the European Space Agency (ESA) mission *Gaia* (https://www.cosmos.esa.int/gaia), processed by the *Gaia* Data Processing and Analysis Consortium (DPAC; https://www.cosmos.esa.int/web/gaia/dpac/consortium). Funding for the DPAC has been provided by national institutions, in particular the institutions participating in the *Gaia* Multilateral Agreement.

SK is partially supported by NSF grants AST-1813881, AST-1909584, and Heising-Simons foundation grant 2018-1030. DB is grateful to Magdalen College for his Fellowship by Examination and the Rudolf Peierls Centre for Theoretical Physics for providing office space and travel funds. TSL and APJ are supported by NASA through Hubble Fellowship grant *HST*-HF2-51439.001 and *HST*-HF2-51393.001, respectively, awarded by the Space Telescope Science Institute, which is operated by the Association of Universities for Research in Astronomy, Inc., for NASA, under contract NAS5-26555. JDS, SLM, and DBZ acknowledge the support of the Australian Research Council (ARC) through Discovery Project grant DP180101791. GSDaC also acknowledges ARC support through Discovery Project grant DP1501013294. Parts of this research were supported by the Australian Research Council Centre of Excellence for All Sky Astrophysics in 3 Dimensions (ASTRO 3D), through project number CE170100013. We also thank the referee Ulrich Heber for a detailed report.

Software: NUMPY (van der Walt, Colbert & Varoquaux 2011), SCIPY (Jones et al. 2001), MATPLOTLIB (Hunter 2007), ASTROPY (Astropy Collaboration et al. 2013; Price-Whelan et al. 2018), EMCEE (Foreman-Mackey et al. 2013), GALA (Price-Whelan 2017), Q3C (Koposov & Bartunov 2006), ISOCHRONES (Morton 2015) FASTKDE (O'Brien et al. 2016), DYNESTY (Speagle 2019), PYMULTINEST (Buchner et al. 2014), IPYTHON (Perez & Granger 2007), CHAINCONSUMER (Hinton 2016), REBOUND (Rein & Liu 2012), MULTINEST (Feroz, Hobson & Bridges 2009), RVSPECFIT (Koposov 2019), SCHWIMMBAD (Price-Whelan & Foreman-Mackey 2017)

## REFERENCES

Abbott T. M. C. et al., 2018, ApJS, 239, 18
Ahn C. P. et al., 2012, ApJS, 203, 21
Anders F. et al., 2019, A&A, 628, A94
Astropy Collaboration et al., 2013, A&A, 558, A33
Barnard E. E., 1916, AJ, 29, 181
Bartko H. et al., 2009, ApJ, 697, 1741
Baumgardt H., Gualandris A., Portegies Zwart S., 2006, MNRAS, 372, 174
Becklin E. E., Neugebauer G., 1968, ApJ, 151, 145
Belokurov V., Koposov S. E., 2016, MNRAS, 456, 602
Bianchi L., Shiao B., Thilker D., 2017, ApJS, 230, 24
Binney J., Tremaine S., 2011, Galactic Dynamics, Vol. 20. Princeton Univ. Press, Princeton, NJ
Blaauw A., 1961, Bull. Astron. Inst. Netherlands, 15, 265
Blaauw A., Morgan W. W., 1954, ApJ, 119, 625
Bland-Hawthorn J., Cohen M., 2003, ApJ, 582, 246
Bonnell I. A., Rice W. K. M., 2008, Science, 321, 1060
Boubert D., Evans N. W., 2016, ApJ, 825, L6
Boubert D., Erkal D., Evans N. W., Izzard R. G., 2017, MNRAS, 469, 2151
Boubert D., Guillochon J., Hawkins K., Ginsburg I., Evans N. W., Strader J., 2018, MNRAS, 479, 2789
Boubert D. et al., 2019, MNRAS, 486, 2618
Bovy J., Rix H.-W., 2013, ApJ, 779, 115

Boyajian T. S. et al., 2013, ApJ, 771, 40
Brent R. P., 1973, Algorithms for Minimization without Derivatives. Prentice-Hall, Englewood, NJ
Bromley B. C., Kenyon S. J., Geller M. J., Barcikowski E., Brown W. R., Kurtz M. J., 2006, ApJ, 653, 1194
Bromley B. C., Kenyon S. J., Brown W. R., Geller M. J., 2018, ApJ, 868, 25
Brown W. R., 2015, ARA&A, 53, 15
Brown W. R., Geller M. J., Kenyon S. J., Kurtz M. J., 2005, ApJ, 622, L33
Brown W. R., Geller M. J., Kenyon S. J., Kurtz M. J., 2006, ApJ, 647, 303
Brown W. R., Geller M. J., Kenyon S. J., 2009, ApJ, 690, 1639
Brown W. R., Lattanzi M. G., Kenyon S. J., Geller M. J., 2018, ApJ, 866, 39
Buchner J. et al., 2014, A&A, 564, A125
Chabrier G., 2005, in Corbelli E., Palla F., Zinnecker H., eds, Astrophysics and Space Science Library Vol. 327, The Initial Mass Function 50 Years Later, Springer, Dordrecht. p. 41
Choi J., Dotter A., Conroy C., Cantiello M., Paxton B., Johnson B. D., 2016, ApJ, 823, 102
Christlieb N., Beers T. C., Thom C., Wilhelm R., Rossi S., Flynn C., Wisotzki L., Reimers D., 2005, A&A, 431, 143
Contigiani O., Rossi E. M., Marchetti T., 2019, MNRAS, 487, 4025
Dalton G. et al., 2014, SPIE, 9147, 91470L
Darbha S., Coughlin E. R., Kasen D., Quataert E., 2019, MNRAS, 482, 2132
de Jong R. S. et al., 2014, SPIE, 9147, 91470M
DESI Collaboration et al., 2016, preprint (arXiv:1611.00036)
Dopita M. et al., 2010, Ap&SS, 327, 245
Dotter A., 2016, ApJS, 222, 8
Edelmann H., Napiwotzki R., Heber U., Christlieb N., Reimers D., 2005, ApJ, 634, L181
Eggen O. J., 1983, ApJS, 51, 183
Eggen O. J., Greenstein J. L., 1967, ApJ, 150, 927
Eggen O. J., Lynden-Bell D., Sandage A. R., 1962, ApJ, 136, 748
Erkal D., Belokurov V., Bovy J., Sanders J. L., 2016, MNRAS, 463, 102
Erkal D., Boubert D., Gualandris A., Evans N. W., Antonini F., 2019, MNRAS, 483, 2007
Evans D. W. et al., 2018, A&A, 616, A4
Feroz F., Hobson M. P., 2008, MNRAS, 384, 449
Feroz F., Hobson M. P., Bridges M., 2009, MNRAS, 398, 1601
Foreman-Mackey D., Hogg D. W., Lang D., Goodman J., 2013, PASP, 125, 306
Gaia Collaboration et al., 2016, A&A, 595, A1
Gaia Collaboration et al., 2018, A&A, 616, A1
Genzel R., Eisenhauer F., Gillessen S., 2010, Rev. Mod. Phys., 82, 3121
Ghez A. M., Salim S., Hornstein S. D., Tanner A., Lu J. R., Morris M., Becklin E. E., Duchêne G., 2005, ApJ, 620, 744
Gillessen S., Eisenhauer F., Trippe S., Alexander T., Genzel R., Martins F., Ott T., 2009, ApJ, 692, 1075
Gillessen S. et al., 2017, ApJ, 837, 30
Gnedin O. Y., Gould A., Miralda-Escudé J., Zentner A. R., 2005, ApJ, 634, 344
Goodman J., Weare J., 2010, CAMCS, 5, 65
Gravity Collaboration et al., 2018, A&A, 615, L15
Gravity Collaboration et al., 2019, A&A, 625, L10
Greenstein J. L., Sargent A. I., 1974, ApJS, 28, 157
Gualandris A., Merritt D., 2009, ApJ, 705, 361
Gualandris A., Portegies Zwart S., 2007, MNRAS, 376, L29
Guo F., Mathews W. G., 2012, ApJ, 756, 181
Hattori K., Valluri M., Bell E. F., Roederer I. U., 2018a, ApJ, 866, 121
Hattori K., Valluri M., Castro N., 2018b, ApJ, 869, 33
Heber U., Edelmann H., Napiwotzki R., Altmann M., Scholz R.-D., 2008, A&A, 483, L21
Hills J. G., 1988, Nature, 331, 687
Hinton S. R., 2016, JOSS, 1, 00045
Hirsch H. A., Heber U., O'Toole S. J., Bresolin F., 2005, A&A, 444, L61
Huang Y. et al., 2017, ApJ, 847, L9
Hunter J. D., 2007, CSE, 9, 90
Husser T.-O., Wende-von Berg S., Dreizler S., Homeier D., Reiners A., Barman T., Hauschildt P. H., 2013, A&A, 553, A6
Irrgang A., Kreuzer S., Heber U., 2018, A&A, 620, A48
Irrgang A., Geier S., Heber U., Kupfer T., Fürst F., 2019, A&A, 628, L5
Jones E., Oliphant T., Peterson P. et al., 2001, SciPy: Open Source Scientific Tools for Python. Available at: http://www.scipy.org/
Kafle P. R., Sharma S., Lewis G. F., Bland-Hawthorn J., 2014, ApJ, 794, 59
Keenan P. C., Keller G., 1953, ApJ, 117, 241
Kennedy P. M., Przybylski A., 1963, MNRAS, 126, 381
Koposov S., 2019, RVSpecFit: Radial Velocity and Stellar Atmospheric Parameter Fitting. ascl:1907.013
Koposov S., Bartunov O., 2006, in Gabriel C., Arviset C., Ponz D., Enrique S., eds, ASP Conf. Ser. Vol. 351, Astronomical Data Analysis Software and Systems XV. Astron. Soc. Pac., San Francisco, p. 735
Koposov S. E. et al., 2011, ApJ, 736, 146
Koposov S. E., Belokurov V., Torrealba G., 2017, MNRAS, 470, 2702
Launhardt R., Zylka R., Mezger P. G., 2002, A&A, 384, 112
Levin Y., 2006, ApJ, 653, 1203
Levin Y., Beloborodov A. M., 2003, ApJ, 590, L33
Lewis I. J. et al., 2002, MNRAS, 333, 279
Li Y.-B. et al., 2018, AJ, 156, 87
Lindegren L. et al., 2018, A&A, 616, A2
Li T. S. et al., 2019, MNRAS, 490, 3508
LSST Science Collaboration et al., 2009, preprint (arXiv:0912.0201)
Lu Y., Zhang F., Yu Q., 2010, ApJ, 709, 1356
Lucas W. E., Bonnell I. A., Davies M. B., Rice W. K. M., 2013, MNRAS, 433, 353
Luyten W. J., 1979, New Luyten catalogue of stars with proper motions larger than two tenths of an arcsecond; and first supplement; NLTT. (Minneapolis (1979)); Label 12 = short description; Label 13 = documentation by Warren; Label 14 = catalogue
Lu J. R., Do T., Ghez A. M., Morris M. R., Yelda S., Matthews K., 2013, ApJ, 764, 155
Madigan A.-M., Levin Y., Hopman C., 2009, ApJ, 697, L44
Marchetti T., Rossi E. M., Brown A. G. A., 2018, MNRAS, 2466
Martin D. C. et al., 2005, ApJ, 619, L1
Massey P., Levine S. E., Neugent K. F., Levesque E., Morrell N., Skiff B., 2018, AJ, 156, 265
McMillan P. J., 2017, MNRAS, 465, 76
Moe M., Di Stefano R., 2013, ApJ, 778, 95
Morton T. D., 2015, Astrophysics Source Code Library, record ascl:1503.010
Navarro J. F., Frenk C. S., White S. D. M., 1997, ApJ, 490, 493
Nayakshin S., Cuadra J., Springel V., 2007, MNRAS, 379, 21
O'Brien T. A., Kashinath K., Cavanaugh N. R., Collins W. D., O'Brien J. P., 2016, Comput. Stat. Data Anal., 101, 148
O'Leary R. M., Loeb A., 2008, MNRAS, 383, 86
Oort J. H., 1926, PhD thesis, Publications of the Kapteyn Astronomical Laboratory Groningen
Paumard T. et al., 2006, ApJ, 643, 1011
Perez F., Granger B. E., 2007, CSE, 9, 21
Poveda A., Ruiz J., Allen C., 1967, BOTT, 4, 86
Price-Whelan A. M., 2017, J. Open Source Softw., 2, 388
Price-Whelan A. M., Foreman-Mackey D., 2017, J. Open Source Softw., 2, 357
Price-Whelan A. M. et al., 2018, AJ, 156, 123
Przybilla N., Nieva M. F., Heber U., Firnstein M., Butler K., Napiwotzki R., Edelmann H., 2008, A&A, 480, L37
Raghavan D. et al., 2010, ApJS, 190, 1
Rasskazov A., Fragione G., Leigh N. W. C., Tagawa H., Sesana A., Price-Whelan A., Rossi E. M., 2019, ApJ, 878, 17
Rein H., Liu S.-F., 2012, A&A, 537, A128
Schlegel D. J., Finkbeiner D. P., Davis M., 1998, ApJ, 500, 525
Schönrich R., Binney J., Dehnen W., 2010, MNRAS, 403, 1829
Sesana A., Haardt F., Madau P., 2007, MNRAS, 379, L45
Sharp R. et al., 2006, in McLean I. S., Iye M., eds, Proc. SPIE Conf. Ser. Vol. 6269, Ground-based and Airborne Instrumentation for Astronomy. SPIE, Bellingham, p. 62690G

Shen K. J. et al., 2018, ApJ, 865, 15
Sherwin B. D., Loeb A., O'Leary R. M., 2008, MNRAS, 386, 1179
Shipp N. et al., 2018, ApJ, 862, 114
Skrutskie M. F. et al., 2006, AJ, 131, 1163
Speagle J. S., 2019, preprint (arXiv:1904.02180)
Su M., Slatyer T. R., Finkbeiner D. P., 2010, ApJ, 724, 1044
Tauris T. M., 2015, MNRAS, 448, L6
Trotta R., 2007, MNRAS, 378, 72
van Maanen A., 1917, PASP, 29, 258
van der Walt S., Colbert S. C., Varoquaux G., 2011, CSE, 13, 22
Vegetti S., Lagattuta D. J., McKean J. P., Auger M. W., Fassnacht C. D., Koopmans L. V. E., 2012, Nature, 481, 341
Verdinelli I., Wasserman L., 1995, J. Am. Stat. Assoc., 90, 614
Vickers J. J., Grebel E. K., Huxor A. P., 2012, AJ, 143, 86
Weiler M., 2018, A&A, 617, A138
Wolf C. et al., 2018, PASA, 35, e010
Wright E. L. et al., 2010, AJ, 140, 1868
Yanny B. et al., 2000, ApJ, 540, 825
Yanny B. et al., 2009, AJ, 137, 4377
Yelda S., Ghez A. M., Lu J. R., Do T., Meyer L., Morris M. R., Matthews K., 2014, ApJ, 783, 131
Yoon J. H., Johnston K. V., Hogg D. W., 2011, ApJ, 731, 58
York D. G. et al., 2000, AJ, 120, 1579
Yu Q., Madau P., 2007, MNRAS, 379, 1293
Yu Q., Tremaine S., 2003, ApJ, 599, 1129
Zhang F., Lu Y., Yu Q., 2010, ApJ, 722, 1744
Zheng Z. et al., 2014, ApJ, 785, L23
Zubovas K., King A. R., Nayakshin S., 2011, MNRAS, 415, L21

[1]*McWilliams Center for Cosmology, Carnegie Mellon University, 5000 Forbes Ave, Pittsburgh, PA 15213, USA*
[2]*Institute of Astronomy, University of Cambridge, Madingley Road, Cambridge CB3 0HA, UK*
[3]*Magdalen College, University of Oxford, High Street, Oxford OX1 4AU, UK*
[4]*Observatories of the Carnegie Institution for Science, 813 Santa Barbara Street, Pasadena, CA 91101, USA*
[5]*Department of Astrophysical Sciences, Princeton University, Princeton, NJ 08544, USA*
[6]*Fermi National Accelerator Laboratory, PO Box 500, Batavia, IL 60510, USA*
[7]*Kavli Institute for Cosmological Physics, University of Chicago, Chicago, IL 60637, USA*
[8]*Department of Physics, University of Surrey, Guildford GU2 7XH, UK*
[9]*Research School of Astronomy and Astrophysics, Australian National University, Canberra, ACT 2611, Australia*
[10]*Department of Physics, Astronomy, Macquarie University, Sydney, NSW 2109, Australia*
[11]*Macquarie University Research Centre for Astronomy, Astrophysics, Astrophotonics, Sydney, NSW 2109, Australia*
[12]*Lowell Observatory, 1400 W Mars Hill Rd, Flagstaff, AZ 86001, USA*
[13]*Australian Astronomical Optics, Faculty of Science and Engineering, Macquarie University, Macquarie Park, NSW 2113, Australia*
[14]*Sydney Institute for Astronomy, School of Physics, A28, The University of Sydney, NSW 2006, Australia*
[15]*Centre of Excellence for All-Sky Astrophysics in Three Dimensions (ASTRO 3D), Australia*
[16]*School of Physics, UNSW, Sydney, NSW 2052, Australia*
[17]*Department of Astronomy, Astrophysics, University of Chicago, 5640 S Ellis Avenue, Chicago, IL 60637, USA*
[18]*George P. and Cynthia Woods Mitchell Institute for Fundamental Physics and Astronomy, Department of Physics and Astronomy, Texas A&M University, College Station, TX 77843, USA*

This paper has been typeset from a TEX/LATEX file prepared by the author.